Non-ohmic resistance of multiple ion-exchange membranes in series

Z.N. Kramer

TU Delft

Non-ohmic resistance of multiple ion-exchange membranes in series

by

Z.N. Kramer

to obtain the degree of Master of Science
at the Delft University of Technology,
to be defended publicly on Tuesday August 16, 2022 at 14:00 PM.

Student number:	4365321	
Project duration:	December 13, 2021 – August 16, 2022	
Thesis committee:	Dr. E.M. Kelder,	TU Delft, supervisor
	Dr. ir. D.A. Vermaas,	TU Delft
	Dr. ir. J.W. Haverkort,	TU Delft
Daily supervisor:	ir. S. den Haan,	AquaBattery

TU Delft

Preface

For the past couple of years, I have been very interested in energy storage. I think energy storage is the missing key for the energy transition. During my MSc Thesis, I wanted to obtain more knowledge about a specific energy storage system and contribute something to this technology. Fortunately, I came in contact with AquaBattery and after an exciting conversation with ir. Samir den Haan and ir. Emil Goossen, I found myself a great graduation company. After I contacted Dr. Erik Kelder about this opportunity and he saw the potential of this research, my MSc Thesis kicked off.

Since I have a bachelors in Mechanical Engineering, I had no prior experience with membrane or flow battery technology. However, I was able to tackle the challenges on my way and I was glad to be able to design and build my own flowframe testing stack.

This report is written as a MSc Thesis, assuming the reader has basic knowledge of ion-exchange membranes and electrochemistry. Readers that are particularly interested in the effect of different current densities on the (non-)ohmic resistance of ion-exchange membranes, can find this information in section 4.1. Readers who are more interested in (non-)ohmic resistance of ion-exchange membranes in series, can find this information in section 4.4.

I would like to thank my supervisor Dr. Erik Kelder for his advice and flexibility during this project and Dr. ir. David Vermaas and Dr. ir. Willem Haverkort, for accepting my invitation of being my MSc thesis committee and taking time to read and grade this report. I want to give my biggest thank you to ir. Samir den Haan for his outstanding help and thinking along. The colleagues of AquaBattery and especially Dr. Kaustub Singh cannot go unmissed in this preface and I would like to thank all of them for their help, interesting lunch topics and their genuine interest. I want to thank my girlfriend, Vera, for her utmost help and patience during my thesis project. Thanks to Kars and the rest of my friends and family, who supported me not only during my thesis, but also during my past couple of years.

I would like to end by thanking my mother, who is very proud of me and would have loved to see me graduate but unfortunately passed away a few years back.

Z.N. Kramer
Delft, January 2013

Abstract

This research aims to analyse the non-ohmic resistance of multiple ion-exchange membranes (IEM) in series, for a better understanding of membrane resistances. These membranes can be found in series in energy storage systems such as acid-base flow batteries (ABFB).

The effect of different current densities on the ohmic and non-ohmic resistance of bipolar membranes (BPM), under forward and reverse bias were studied using electrochemical impedance spectroscopy (EIS). Hereafter, an anion exchange membrane (AEM), cation exchange membrane (CEM) and BPM were examined individually and in series using EIS, to compose a simplified equivalent circuit for a whole ABFB triplet.

For the effect of different current densities on the BPM, an exponential decline of the non-ohmic resistance of the diffusion boundary layer (DBL) was found as a function of the current density. Under forward bias, the DBL resistance becomes significant. The resistance of the water dissociation reaction (WDR) was minimal under all current densities. Flow experiments validate a depletion and enrichment of the DBL during water association and dissociation, respectively. To compose a simplified equivalent circuit for an AEM, BPM and CEM in series, it was found that the specific resistances of all membranes can be summed at their respective frequencies. This made it possible to construct a simplified equivalent circuit for a whole triplet containing an AEM, BPM and CEM.

Keywords
Electrochemical impedance spectroscopy, ion exchange membranes, acid-base flow batteries, bipolar membrane, membrane resistance, diffusion boundary layer, membrane characterisation, equivalent circuit model.

Z.N. Kramer, Master Thesis, 2022, Delft University of Technology.

Contents

List of Figures

List of Tables

List of Symbols

Symbol	Description	Unit
E^0	Standard potential at 298K	V
ΔG^0	Standard Gibbs free energy	J
R	Universal gas constant	$\mathrm{Jmol^{-1}K^{-1}}$
ΔG	Gibbs free energy	J
F	Faraday's constant	$\mathrm{Cmol^{-1}}$
n	Number of electrons per reaction	
η_i	Electrochemical potential of component i	$\mathrm{Jmol^{-}1}$
$\mu^0{}_\mathrm{i}$	Standard chemical potential of component i	$\mathrm{Jmol^{-}1}$
P	Pressure	Pa
P^0	Pressure at standard conditions	Pa
ϕ	Electric potential	V
a	Thermodynamic activity of components	
V	Volume	$\mathrm{m^3}$
ϕ_Donnan	Donnan electric potential	V
z_i	Charge sign	
m	Molarity	mol/L
E_i	Electric potential	V
U_i	Potential	V
R	Resistance	Ω
R_DBL	Resistance Diffusion Boundary Layer	Ωcm^2
R_DL	Resistance Double Layer	Ωcm^2
R_Ω	Resistance of ohmic parts	Ωcm^2
R_WDR	Resistance Water Dissociation Reaction	Ωcm^2
C	Capacitance	F
Q	Constant Phase Element	Fs^n
Q_DL	Constant Phase Element of Double Layer	Fs^n
Q_DBL	Constant Phase Element of Diffusion Boundary Layer	Fs^n
I	Current	A
ω	Angular velocity	$\mathrm{rads^{-1}}$
t	Time	s
φ	Phase shift	rad
Z	Impedance	Ω
Z'	Real Impedance	Ω
Z''	Imaginary Impedance	Ω
j	Complex number	
k	Stiffness	N/m
E	Young's modulus	Pa
L	Length	m
F_axial	Force in axial direction	N
T	Torque	Nm
d	Diameter	m
Re	Reynolds number	
ρ	Density	$\mathrm{kg/m^3}$
μ	Dynamic velocity	$\mathrm{kg/(m*s)}$

List of Abbreviations

EIS Electrochemical Impedance Spectroscopy

AC Alternating Current

DC Direct Current

CPE Constant Phase Element

LCOE Levelised Costs Of Electricity

ESS Energy Storage Systems

PHS Pumped Hydro Storage

ABFB Acid-Base Flow Battery

IEM Ion-Exchange Membrane

MPM Monopolar Membrane

AEM Anion Exchange Membrane

CEM Cation Exchange Membrane

BPM Bipolar Membrane

AEL Anion Exchange Layer

CEL Cation Exchange Layer

NHE Normal Hydrogen Electrode

SHE Standard Hydrogen Electrode

OCV Open Circuit Voltage

PEEK Polyetheretherketone

ED Electrodialysis

RED Reverse Electrodialysis

SOC State Of Charge

SOH State Of Health

SEI Solid Electrolyte Interface

DBL Diffusion Boundary Layer

DL Double Layer

IL Inter Layer

WDR Water Dissociation Reaction

1 Introduction

Energy storage in batteries is a cost-effective key ingredient for the energy transition [51] [74] [19]. Whilst the penetration of renewable energy rapidly increases, the energy grid is shaking on its foundation [3] [63].

The evidence of the connection between greenhouse gas emissions and climate change are undisputed [5]. Last century, the CO_2 emissions from energy combustion and industrial processes multiplied by a factor 10, as Figure 1.1 shows [2].

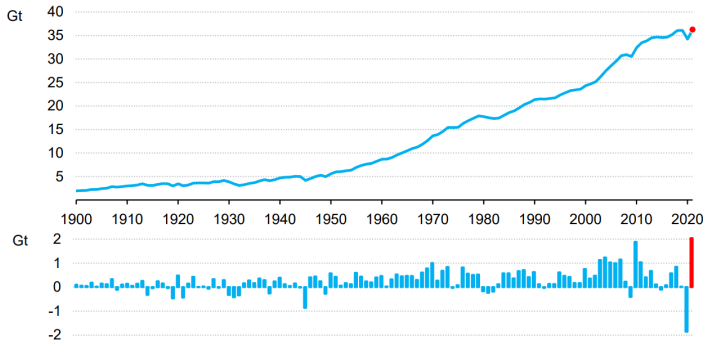

Figure 1.1: Total CO_2 emissions from energy combustion and industrial processes and their annual change, 1900-2021 [2]

Electricity and heat production is the source of more than 40% of the global CO_2 emissions [1]. To achieve the legally binding international goals of the 2015 Paris Agreement [55], the EU greenhouse gas emissions have to decrease by at least 55% by 2030 compared to the emissions in 1990 [15]. This goal can only be achieved if the energy transition will take place.

At this moment, solar and wind energy constitute the major components of the renewable power generation [54]. The last two decades, solar and wind technologies have experienced a rapid decline in their costs. Currently, their levelised costs of electricity (LCOE) are lower than those of fossil fuel technologies [75].

However, in contrast to burning fossil fuels, renewable energy sources are intermittent and uncontrollable in terms of timing [57] [44] [63]. Wind energy can only generate energy when the wind blows and solar energy can only be harvested depending on hourly, daily, and seasonal conditions [3] [69]. This intermittent behaviour of renewable energy sources nourishes the need for more flexible energy sources in the future energy mix. Currently, this flexibility is provided by gas turbines and coal plants [43]. Because of the depletion of fossil fuels, the impact of greenhouse gas emitting power sources and the inflation makes fossil energy more expensive, the demand for energy storage systems (ESS) is increasing rapidly [32]. This flexibility in power systems can only be achieved when the energy generation and demand become more flexible with storage systems acting as mediators to manage their

interconnection [32].

For a proper renewable energy system, two types of energy storage are required: short-term energy storage and long-term energy storage. Short-term energy storage is considered as energy storage lasting seconds to several hours. Long-term energy storage is considered as energy storage for more than several hours [63]. Since renewables often have distinct daily and seasonal variations, there is especially a need for long-term energy storage [63].

The past couple of decades, a number of technology's available for energy storage have arised. However, only a few of them are commercially deployed. In Figure 1.2 [63], an overview of energy storage systems is given with a comparison of conceptual discharge time and power range, based on findings of Chen et al. [13]. At this moment, pumped hydro energy storage (PHS) is the most mature long-term energy storage system and the only technology available at large scale [63]. However, PHS also has geographical limitations as it needs to store massive amount of water at elevated heights.

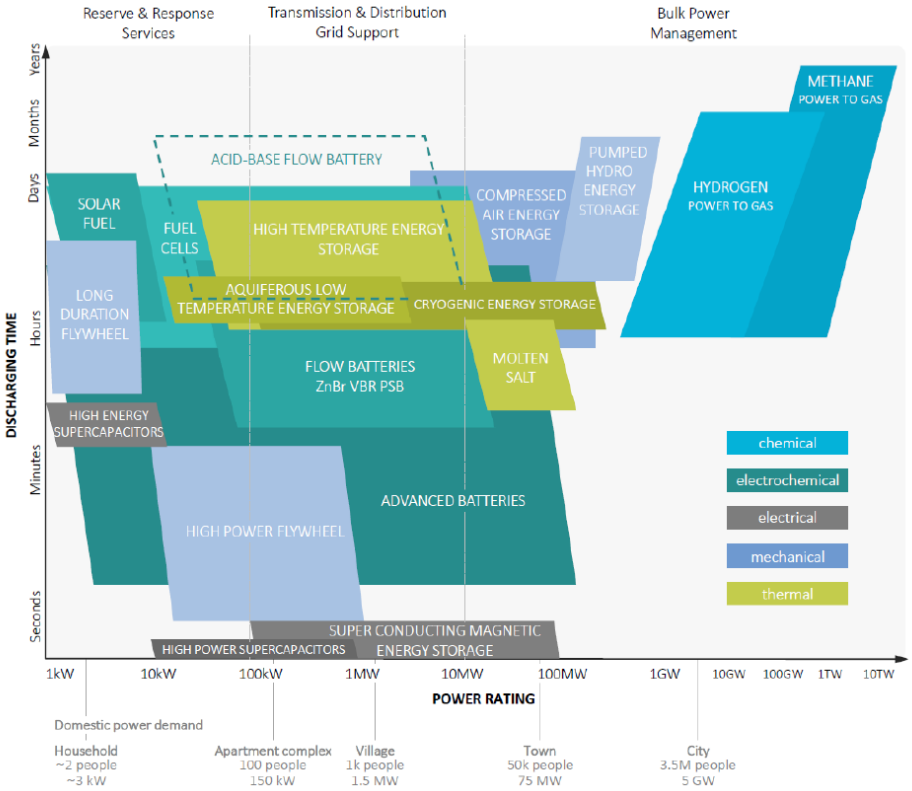

Figure 1.2: Simplified schematic overview of energy storage technologies, compared by conceptual discharge time and power range. The domestic power demand scale is based on the peak electric load demand of 3 kW per average EU household (≈ 2 people). [63]

The acid-base flow battery (ABFB) can become an innovative, safe and sustainable storage system since it can provide long-term storage for reserve and response services and grid support [27]. The benefits of the ABFB are that power and capacity can be scaled independently from each other, the materials are abundantly available and environmentally friendly [63] [21].

The ABFB can be considered as an alteration to the concentration gradient flow battery [28]. For an ABFB, the system stores electricity in aqueous fluids based on water and table salt (NaCl). Using membrane technology and applying an electrical field, the ions in this salt solution are separated and water gets dissociated into H^+ and OH^- ions [17]. The final energy containing solutions are an acid and base solution [21].

Three different ion-exchange membranes (IEM) are used in the ABFB; two monopolar membranes (MPM) and one bipolar membrane (BPM). The used MPM are an anion exchange membrane (AEM) and a cation exchange membrane (CEM). These monopolar membranes are designed to let specifically charged ions pass, whilst blocking other ions. The BPM is designed to dissociate water into H^+ and OH^-

ions and associate vice-versa. These membranes have equivalent electrical circuits, consisting out of different parts of the membrane and the membrane-solution interface [60] [9]. The resistances of these membranes have an ohmic and a non-ohmic part (constant phase element or non-ideal capacitor), due to the interfaces [9].

In previous research, Park et al. [60] [61] and Blommaert et al. [9] use Electrochemical Impedance Spectroscopy (EIS) to identify the (non-)ohmic resistance of different parts of the membrane to their equivalent electrical circuit. However, multiple ion-exchange membranes in series for an ABFB and the contribution of multiple membranes to the non-ohmic resistances have not been analysed before.

The aim of this research is to analyse the non-ohmic resistance of multiple ion-exchange membranes in series. To find the answer to this aim, the following two sub-questions are formulated:

1. **What is the effect of different current densities on the ohmic and non-ohmic resistance of bipolar membranes, under forward and reverse bias for electrochemical impedance spectroscopy?**
2. **Is it possible to compose a simplified equivalent circuit of multiple ion-exchange membranes in series, by using Electrochemical Impedance Spectroscopy data?**

This report will be presented in the following structure. In chapter 2 the theoretical background information on the ABFB will be provided. The methodology of this research will be located in chapter 3. The results and discussion can be found in chapter 4. Finally, chapter 5 concludes this research and provides some future recommendations.

2

Theoretical Background

In this chapter, the literature is discussed that is of value for this thesis. This includes the basics of electrochemistry in section 2.1, ion-exchange membranes in section 2.2, the Acid-Base flow battery in section 2.3 and Electrochemical Impedance Spectroscopy in section 2.4.

2.1. Electrochemistry

Electrochemistry focuses on the interrelation of electrical and chemical effects. In electrochemistry, the overall chemical reaction is made up of two independent half-reactions, including electrons and chemical species [6]. For a water dissociation reaction as shown in Equation 2.1, two half reactions can be formed. The half reactions described in Equation 2.2 and Equation 2.3, shows us the half-reactions of dissociating water into H^+ and OH^- [39] [88].

$$H_2O \rightleftarrows H^+ + OH^- \tag{2.1}$$

$$2H^+ + 2e^- \rightarrow H_2 \qquad E^0 = 0.000V \tag{2.2}$$

$$2H_2O + 2e^- \rightarrow H_2 + 2OH^- \qquad E^0 = -0.828V \tag{2.3}$$

The reaction in Equation 2.3, has a standard potential of $E^0 = -0.828V$. Standard potential means that the potential of the reaction at the standard conditions is a relative potential to the standard electrode potential, which contain solutions with concentrations of 1 M and pressures of 1 atm. This standard electrode potential is called normal hydrogen electrode (NHE) or standard hydrogen electrode (SHE) [49] [14].

In general, the reaction of Equation 2.3 can be described as the reduction reaction of Equation 2.4. Here, O is the oxidised species, R is the reduced species and n is the number of electrons exchanged between O and R. From this equation the Gibbs free energy change (ΔG) can be derived, as shown in Equation 2.5. In this equation, $[O]$ and $[R]$ are the concentrations of both the components, R is the gas constant ($8.3145 Jmol^{-1}K^{-1}$) and T is the temperature in Kelvin [14].

$$O + ne^- \rightleftarrows R \tag{2.4}$$

$$\Delta G = \Delta G^0 + RTln\frac{[R]}{[O]} \tag{2.5}$$

In the end, the electric potential of a reaction can be calculated using Equation 2.6. E is the maximum potential between two electrodes, also known as OCV (open circuit voltage) and F is Faraday's constant ($F = 96,485.3 Cmol^{-1}$) [14] [72].

$$\Delta G = -nFE \tag{2.6}$$

2.1.1. Nernst equation

In order to determine the potential between two solutions in case of non-standard conditions (pure liquids, 1.0 M solutions and pressure of 1.0 atm), the Nernst equation can be used [39].
By combining Equation 2.5 and Equation 2.6, the Nernst equation of Equation 2.7 can be constructed [14]. In this equation, the actual potential (E) can be derived from the standard potential (E_0).

$$E = E^0 + \frac{RT}{nF} ln \frac{[O]}{[R]} \tag{2.7}$$

For a general half-reaction under different concentrations, as in Equation 2.8, the potential can be determined by the Nernst equation [39].

$$aA + bB + ne^- \rightarrow cC + dD \tag{2.8}$$

The Nernst equation, stated in Equation 2.9, provides the actual potential (E) from the standard potential (E^0) and the molarities or pressures in atmospheres [39]. Using this Nernst equation, the cell potential can be determined.

$$E = E^0 - \frac{0.0592}{n} log \frac{[C]^c[D]^d}{[A]^a[B]^b} \tag{2.9}$$

2.2. Ion-Exchange Membranes

To only let specific charged particles pass, whilst keeping two solutions separate from each other, ion-exchange membranes (IEM) can be used [18]. Ion-Exchange Membranes (IEM) are made out of a polymeric backbone with charged ion groups [87] [18] [41]. An IEM lets specific charged ions through, whilst blocking other ions. Mass transport through a membrane can be induced in four ways: by an electric field or by a concentration, pressure or temperature gradient [64].

In this section, different ion-exchange membranes are introduced in subsection 2.2.1, the permselectivity and potential of membranes are presented in subsection 2.2.2 and membrane-solution interface phenomena are explained in subsection 2.2.3.

2.2.1. Different ion-exchange membranes

There are different kinds of IEM on the market. The monopolar exchange membranes are most common, whilst bipolar membranes are less common. For this research, three different membranes are used.

Anion Exchange Membranes (AEM) are positively charged and are selective permeable for negatively charged ions [77].

Cation Exchange Membranes (CEM) are negatively charged and are selective permeable for positively charged ions [77].

Bipolar Membranes (BPM) consist out of two layers. One Anion Exchange Layer (AEL) and one Cation Exchange Layer (CEL) [20] [65]. The zone between these two layers is referred to as the interlayer (IL) [16]. In theory, no charged particles can pass a BPM, because both positively and negatively charged ions cannot pass through one of the layers [62]. BPM are mainly designed to dissociate water (H_2O) into hydroxide ions (OH^-) and protons (H^+) by exposing it to an electric field (see Figure 2.1 a) [82] [87] [62]. This process is called water dissociation and is not the same as water splitting. Dissociation of water forms H^+ and OH^- ions in an aqueous solution. Water splitting is the process of splitting H_2) into H_2(g) and O_2(g) at the electrodes, whilst water dissociation appears inside the BPM and no gas is formed [62].

This specific reaction inside the bipolar membrane can also be reversed. In this case, hydroxide ions (OH^-) and protons (H^+) associate back into water (H_2O), shown in Figure 2.1 b. According to Blommaert [10], BPMs can have imperfections leading to unwanted behaviour like ion crossover, blistering, high resistance and slow kinetics. Especially the blistering is an unwanted effect that appears in forward bias. If the applied current is too high, too much water is recombined inside the BPM and this will cause blisters in between the layers.

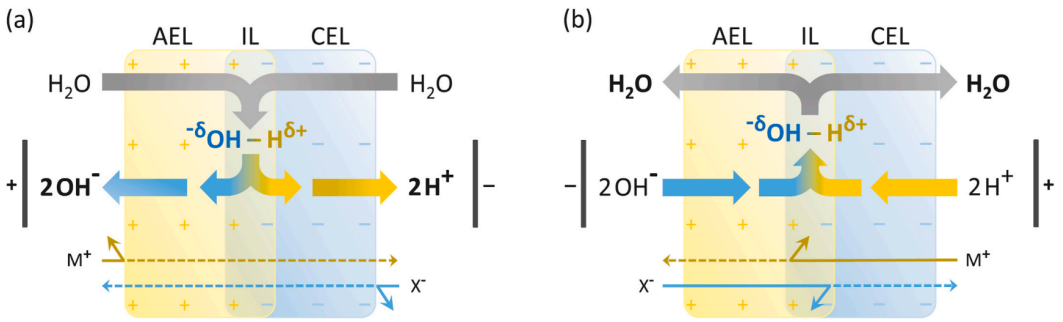

Figure 2.1: Schematic overview of the principle of a BPM. (a) BPM under reverse bias, where first the junction is depleted of ions and then water dissociates into H^+ and OH^- ions; (b) BPM under forward bias, where ions are transported into the membrane and water is formed at the bipolar junction [62]

2.2.2. Permselectivity and potential of membranes

The permselectivity of membranes is the extent of blocking of the membrane towards the passage of counter-ions. This permselectivity is of crucial importance, since it defines the potential over the membrane. When co-ions can also pass the membrane, this potential will decrease [53].

The selective uptake of counter-ions and rejection of co-ions by the charged membrane is explained by a Donnan membrane equilibrium [68] [72]. If electrical potential ϕ is applied to the system, the anion has an electrochemical potential of η_A (Equation 2.10), the cation of η_C (Equation 2.11) and the solvent (water) of η_W (Equation 2.12) [68].

$$\eta_A = \mu^0{}_A + RT\ln a_A + (P - P^0)V_A + z_A F\phi \tag{2.10}$$

$$\eta_C = \mu^0{}_C + RT\ln a_C + (P - P^0)V_C + z_C F\phi \tag{2.11}$$

$$\eta_W = \mu^0{}_W + RT\ln a_W + (P - P^0)V_W \tag{2.12}$$

Here, μ^0 is the chemical potential of the membrane/solvent under standard conditions (1 atm, in pure water), R is the gas constant, T is the temperature (Kelvin), a is the activity of the respective components, P is the pressure, P^0 is the pressure under standard conditions, V is the partial molar volume, z is the valence of the membranes/solvent and F is the Faraday constant ($F = 96,485.3 Cmol^{-1}$).

The Donnan equation is based on the equations of chemical potentials and shown in Equation 2.13. This equation describes an equilibrium with electrical potential ϕ_{Donnan} between two solutions, divided by an IEM [68].

$$\phi_{Donnan} = \bar{\phi} - \phi = \frac{1}{z_i F}\left[RT\ln\frac{a_i}{\bar{a}_i} - (\bar{P} - P)V_i\right] \tag{2.13}$$

In Figure 2.2, a schematic is given of a monopolar membrane (in this case a CEM), immersed in two different electrolytes. In this overview, the electrolyte on the left-hand side is concentrated, whilst the electrolyte on the right-hand side diluted. The black lines are the molarities (m) and the red lines are the potentials (ϕ) [26]. Inside the CEM, the membrane contains next to the mobile ions (Na^+ and Cl^-), also fixed charges.

The concentration of these fixed charges inside the membrane is denoted as X. Between the concentration of ions in the electrolyte phase and the concentration of ions in the membrane phase, an equilibrium will develop, known as the Donnan equilibrium [26]. At the left-hand side of the membrane interface, the Donnan equilibrium is defined as in Equation 2.14 [34] [47].

$$m_+^L m_-^L = m_+^{M,L} m_-^{M,L} \tag{2.14}$$

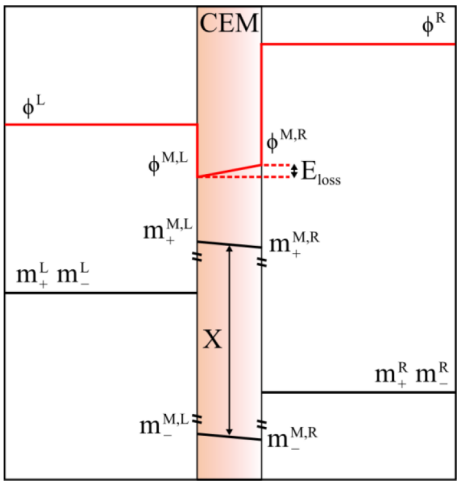

Figure 2.2: Schematic of a CEM, with two different electrolytes. On the left-hand side, the electrolyte is concentrated, whilst on the right-hand side the electrolyte is diluted. The black lines are the molarities (m) and the red lines are potentials (ϕ). [26]

Since the electroneutrality of the membrane should be respected, Equation 2.15 shows this equilibrium. According to Van Egmond [26], Equation 2.16 gives the equation for the co-ion concentration at the left-hand side interface of the CEM if a typical fixed charge concentration value of 5 M is considered.

$$m_+^{M,L} = X + m_-^{M,L} \tag{2.15}$$

$$m_-^{M,L} = \frac{-X + \sqrt{X^2 + 4(m_+^L)^2}}{2} \tag{2.16}$$

The electrical potential of the left side ($E_{\text{Donnan left}}$) is calculated using Equation 2.17. For the right side, a similar calculation can be derived and is shown in Equation 2.18 [26].

$$\phi^{\text{M,L}} - \phi^{\text{L}} = E_{\text{Donnan left}} = \frac{RT}{zF} ln(\frac{m_+^L}{m_+^{M,L}}) \tag{2.17}$$

$$\phi^{\text{R}} - \phi^{\text{M,R}} = E_{\text{Donnan right}} = \frac{RT}{zF} ln(\frac{m_+^{M,R}}{m_+^R}) \tag{2.18}$$

When adding Equation 2.17 and Equation 2.18, inserting Equation 2.15 and Equation 2.16 and rearranging yields the membrane potential based on both Donnan potentials and assuming no diffusion potential is present, Equation 2.19 can be derived [26] [37].

$$E_0 = E_{\text{Donnan left}} + E_{\text{Donnan right}} = \frac{RT}{zF} ln(\frac{m_+^L}{m_+^R} \frac{X + m_-^{M,R}}{X + m_-^{M,L}}) = \frac{RT}{zF} ln(\frac{m_+^L}{m_+^R} \frac{X + \sqrt{X^2 + 4(m_+^R)^2}}{X + \sqrt{X^2 + 4(m_+^L)^2}}) \tag{2.19}$$

2.2.3. Membrane-solution interface phenomena

Adjacent to a membrane, two interacting layers can be identified in the solutions, as shown in Figure 2.3 [77] [90]. In this figure, the ion concentration in and next to the membrane is shown. Because a CEM is shown, the membrane is designed to only let positively charged Na^+ ions through. At the boundaries of the membrane, two interacting layers including a concentration gradient are formed [46].

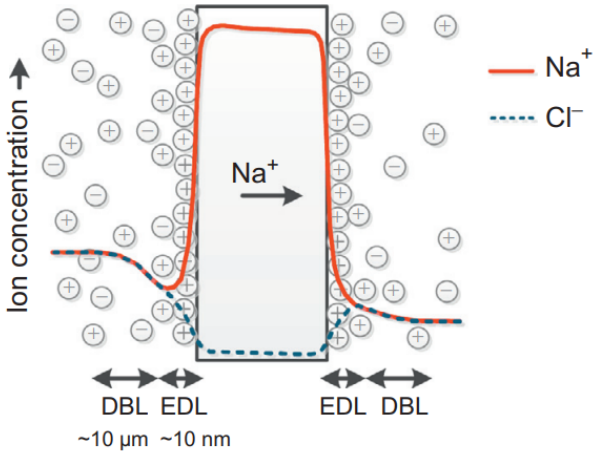

Figure 2.3: Ion concentration and occurring phenomena in the CEM and in the layers adjacent to the membrane in high (left) and low (right) salt concentration compartments. DBL is the diffusion boundary layer and EDL is the electrical double layer. [77]

An electrical double layer (EDL or DL) is formed at nanoscale level, where the concentration of counter ions is significantly larger than that of co-ions [40] [77]. The typical thickness of the EDL is of a few tens of nanometers (Debye length), though the thickness of this layer is dependent on the salt concentration of the solutions (the thickness increases for lower salt concentrations) [77] [23].

A diffusion boundary layer (DBL) forms next to the EDL when ions are transported from a high concentrated salt solution to a lower concentration of salt [77] [35] [40]. Inside the DBL, a concentration gradient is present perpendicular to the membrane [23]. This layer typically has a thickness of hundreds of micrometers in open stirred systems [71], but can be limited to less than 100 micrometers in case of thin feed water compartments with flow [40].

2.3. Acid-base flow battery

In this section, the working principle of the acid-base flow battery (ABFB) is introduced in subsection 2.3.1 and subsection 2.3.2 shows the calculations for the maximum cell potential.

2.3.1. Working principle of the acid-base flow battery

The acid-base flow battery (ABFB) is an electrochemical cell where energy is stored using pH difference between acid and base solutions [26]. This ABFB can be considered as a modification of the flow battery based on concentration gradient. The gradient flow battery relies on electrodialysis (ED) and reverse electrodialysis (RED). In conventional ED, an electric field is applied over a membrane stack that is build out of alternating anion- and cation-exchange membranes (AEM and CEM). By applying an electric field to this stack, the alternating membranes can produce a higher and lower concentration salt stream out of brackish water. The opposite of this reaction is RED. RED uses two streams of different concentrations salt water to force an ion flow through the membranes [8]. This ion flow can be harvested to produce electricity from the two different gradient streams [63].

For an ABFB, a bipolar membrane (BPM) is added to the stack to generate a pH difference between two streams [83]. As stated in section 2.2, bipolar membranes consist out of two oppositely charged layers. Each of the membrane layers could either let positively charged or negatively charged ions pass. In contrast of AEM and CEM, a BPM allows no transport of ions across it. It is designed to

dissociate water at the junction of the two layers [62].

The battery stack of an ABFB consists out of two electrodes in electrolyte, whereafter up to hundreds of so called ”triplets” are placed in between. These triplets always have the same configuration of three different aqueous fluids flowing through spacers and ion-exchange membranes in between. The configuration is as follows: AEM, acid, BPM (CEL towards the acid), base, CEM, salt. Hereafter, this triplet can be repeated to increase the voltage [63].

In Figure 2.4, an overview of a single ABFB triplet stack is given. During charging (Figure 2.4a), an electric field is applied over the stack (also called reverse bias) and inside the BPMs water is dissociated into H^+ and OH^- [63]. In this flow battery triplet, fresh water is pumped in the acid and base channels, whilst salt water (NaCl) is pumped in the salt channel. The salt water is used as a donor fluid, providing Na^+ and Cl^- ions to the acid and base whilst H^+ and OH^- are formed inside the BPM. This principle stores electrical energy by producing acid (HCl) and base (NaOH) solutions and decreases the concentration of NaCl in the salt compartment [63].

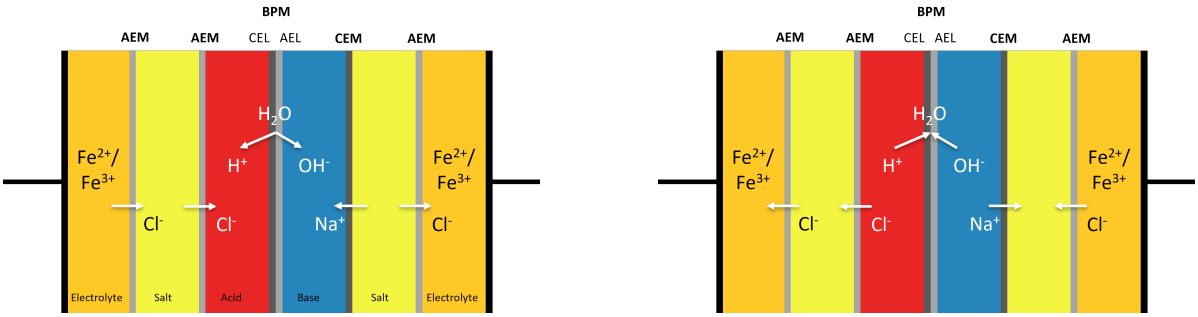

(a) ABFB charging (reverse bias)

(b) ABFB discharging (forward bias)

Figure 2.4: Working principle of an ABFB, charging and discharging (based on [63])

To induce this water dissociation, an electric field of 0.828V per BPM must be applied (at 1M HCl and 1M NaOH) [63]. This is significantly lower than the 1.23V needed for water splitting in conventional electrolysis. The absence of gas production inside the flow battery is also a safety advantage compared to other battery systems based on electrolysis [67].

Harvesting electrical energy from the chemically stored energy can be done by discharging the battery according to Figure 2.4b. Discharging (also called forward bias) the battery means that water is associated inside the BPM and electrons can be harvest at the electrodes. Acid and base are getting neutralised by the extraction of H^+ and OH^- ions into the BPM and Na^+ and Cl^- ions to the salt compartment [63].

Using the three different aqueous fluids and ion-exchange membranes, an ion-flow is forced. In the electrolyte, this ion-flow is converted to an electron-flow by a redox reaction [20].

2.3.2. Cell potential

The maximum cell potential of an acid-base flow battery triplet can be calculated using the Nernst equation of Equation 2.7 in subsection 2.1.1. According to Van Egmond [26], the potential of a whole triplet can be determined by Equation 2.24. This equation consists out of the anion exchange layer (AEL) of the BPM $U_{AEL,\,BPM}$ in Equation 2.20, the cation exchange layer (CEL) of the BPM $U_{CEL,\,BPM}$ in Equation 2.21, the AEM U_{AEM} in Equation 2.22 and the CEM U_{CEM} in Equation 2.23.

For the theoretical potential calculations, 1 M HCl (acid), 1 M NaOH (base) and 0.5 M NaCl (salt) are used in a charged battery. Next to the BPM, acid and base are present, the AEM is between the base and the salt compartments and the CEM is in the middle of the salt and acid compartments. The potential of the AEL and CEL of the BPM is between the acid or base solution and the interface of the

BPM. At the interface of the BPM where both ion exchange materials touch, the concentration of protons and hydroxyl ions is very low (10^{-7} M) [26]. Because the concentration of the protons and hydroxyl ions in the acid and base compartments are much higher (1 M) and due to the Donnan exclusion, a membrane potential is created over each layer of the ion exchange material [26].

$$U_{\text{AEL, BPM}} = \frac{RT}{zF} ln(\frac{[OH^-]_{\text{bp}}}{[OH^-]_{\text{base}}}) \approx \frac{RT}{-F} ln(\frac{10^{-7}}{1}) = 0.414V \tag{2.20}$$

$$U_{\text{CEL, BPM}} = \frac{RT}{zF} ln(\frac{[H^+]_{\text{acid}}}{H^+]_{\text{bp}}}) \approx \frac{RT}{F} ln(\frac{1}{10^{-7}}) = 0.414V \tag{2.21}$$

$$U_{\text{AEM}} = \frac{RT}{zF} ln(\frac{[Cl^-]_{\text{salt}}}{[Cl^-]_{\text{acid}}}) \approx \frac{RT}{-F} ln(\frac{0.5}{1}) = 0.0178V \tag{2.22}$$

$$U_{\text{CEM}} = \frac{RT}{zF} ln(\frac{[Na^+]_{\text{base}}}{[Na^+]_{\text{salt}}}) \approx \frac{RT}{F} ln(\frac{1}{0.5}) = 0.0178V \tag{2.23}$$

$$U_{\text{cell}} = U_{\text{AEL, BPM}} + U_{\text{CEL, BPM}} + U_{\text{AEM}} + U_{\text{CEM}} = 0.864V \tag{2.24}$$

The total maximum cell potential is calculated in Equation 2.24, and is the sum of all four membrane components of the triplet. In case that more than one triplet is used, the maximum triplet potential can be multiplied by the amount of triplets in the stack.

2.4. Electrochemical Impedance Spectroscopy

This section explains the Electrochemical Impedance Spectroscopy measurement method. In subsection 2.4.1, a general introduction of EIS is given, subsection 2.4.2 and subsection 2.4.3 respectively give the equivalent electric circuits of monopolar and bipolar membranes and subsection 2.4.4 shows the effect on the equivalent circuit of multiple membranes in series.

2.4.1. General introduction EIS

Electrochemical Impedance Spectroscopy (EIS) is a method to measure individual components in a system, by examining the electronic responses at different frequencies [6]. EIS can be used to characterise electrodes, interfaces and material properties, to assess the State Of Charge (SOC) and State Of Health (SOH) of rechargeable batteries, modules or packs and the SOH and degradation in supercapacitors and fuel cells [76].

Electrical resistance is the ability of a circuit element to resist the flow of electrical current. This can easily be measured using a DC resistance measurement device. An electrical resistance follows Ohm's law at all current and voltage levels (Equation 2.25). Its resistance value is independent of frequency and alternating currents (AC) and voltage signals through a resistor are in phase with each other [38].

$$R = \frac{E}{I} \tag{2.25}$$

However, many circuit elements in the real world exhibit a more complex behaviour. This complex behaviour forces us to abandon the simple concept of resistance and lets us turn to impedance. Impedance is a measure of the ability of a circuit to resist the flow of electrical current, but it is not limited to the simplifying properties of ohmic resistance [38].

Whilst performing EIS, an alternating current precisely activates processes with a given characteristic time. This allows one to detect individual process contributors as ohmic resistance, interfacial charge-transfer resistance, mass transport resistances in the catalyst layer and back-diffusion layer, in a relatively short measurement time [76].

Electrochemical impedance spectroscopy is a technique that applies an AC signal and measures the response of the circuit [59] [38]. The voltage response (Equation 2.26) of the system is measured after applying an alternating current Equation 2.27 [61].

$$v(t) = v_0 e^{\mathrm{i}(\omega\, \mathrm{t} - \varphi)} \tag{2.26}$$

$$i(t) = i_0 e^{\mathrm{j}\omega\, \mathrm{t}} \tag{2.27}$$

where i_0 is the initially known amplitude, the angular frequency is $\omega = 2\pi f$, where f is the frequency in Hz and $j = \sqrt{-1}$.

In Figure 2.5, a purely sinusoidal voltage v is expressed as Equation 2.28 and a current response i is shown as Equation 2.29 in a representation of a phasor [6]. This current response has a phase shift φ and can be analysed as a sum of sinusoidal functions (a Fourier series) [38].

$$e = Esin\omega t \tag{2.28}$$

$$i = Isin(\omega t + \varphi) \tag{2.29}$$

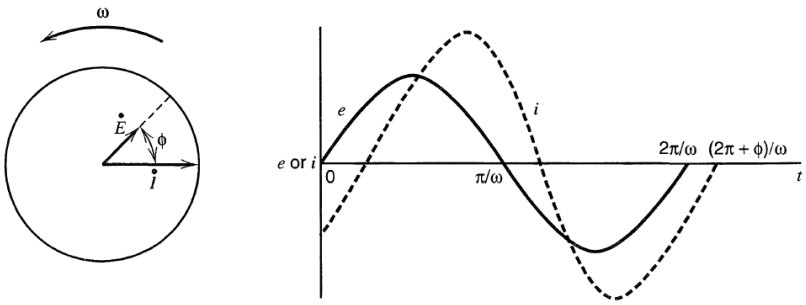

Figure 2.5: Phaser diagram for an alternating voltage including a phase shift. [6]

To acquire the impedance of the system, Z is defined as the ratio of the Laplace Transforms of $v(t)$ and $i(t)$ according to Equation 2.30 [61] [23]. Here, $|Z|$ is the impedance magnitude (v_0/i_0) and φ is the phase difference between the voltage and current.

$$Z = \frac{v_0 e^{\mathrm{j}\varphi}}{i_0} = |Z|e^{\mathrm{j}\varphi} = |Z|cos\varphi - j|Z|sin\varphi \tag{2.30}$$

The impedance Z represents the ratio of the phasor voltage V to the phasor current I, measured in ohms (Ω). For a resistor, inductor, capacitor and constant phase element (CPE), the impedance Z is shown in Equation 2.31, Equation 2.32, Equation 2.33 and Equation 2.34 [4] [23] [38].

$$Resistor: Z = R \tag{2.31}$$

$$Inductor: Z = j\omega L \tag{2.32}$$

$$Capacitor: Z = \frac{1}{j\omega C} \tag{2.33}$$

$$CPE: Z = \frac{1}{(j\omega)^{\mathrm{n}} Q} \tag{2.34}$$

Here, ω is the angular velocity ($1rad/s$), Q is the CPE, with the units Ss^{n}, where S represents Siemens ($\frac{1}{\Omega}$) [23]. The fitting parameter n is an empirical parameter between $0 \leq n \leq 1$. If $n = 0.5$, the element circuit is a Warburg impedance, but if $n = 1$, the circuit is equal to a capacitor [7].

In equivalent circuits, often more than one element is present. Such a system of multiple circuit elements can be calculated. If circuit elements are placed in series, the impedances can be summed as Equation 2.35 describes. The total impedance for a resistance and a capacitance (RC circuit) in series is described in Equation 2.36 [23].

An RC circuit in series can also be plotted in a Nyquist plot, as shown in Figure 2.6a. In this plot, the horizontal axis is the real part (Z_{Re} [Ω]) and the vertical axis is the imaginary part (Z_{Im} [Ω]) [6].

$$Z_{\text{total}} = Z_1 + Z_2 + ... + Z_{\text{n}} \tag{2.35}$$

$$Z_{\text{total}}(\omega) = R + \frac{1}{j\omega C} \tag{2.36}$$

In case different circuit elements are connected parallel to each other, Equation 2.37 shows the calculation of total impedance [23]. For a resistance and capacitance placed in parallel, the total impedance is given by Equation 2.38.

The Nyquist plot for an RC circuit in parallel is shown in Figure 2.6b. For this plot, the horizontal axis is the real part (Z_{Re} [Ω]) and the vertical axis is the imaginary part (Z_{Im} [Ω]) [6].

$$\frac{1}{Z_{\text{total}}} = \frac{1}{Z_1} + \frac{1}{Z_2} + ... + \frac{1}{Z_{\text{n}}} \tag{2.37}$$

$$Z_{\text{total}}(\omega) = \frac{R}{1 + \omega^2 R^2 C^2} - j\frac{\omega R^2 C}{1 + \omega^2 R^2 C^2} \tag{2.38}$$

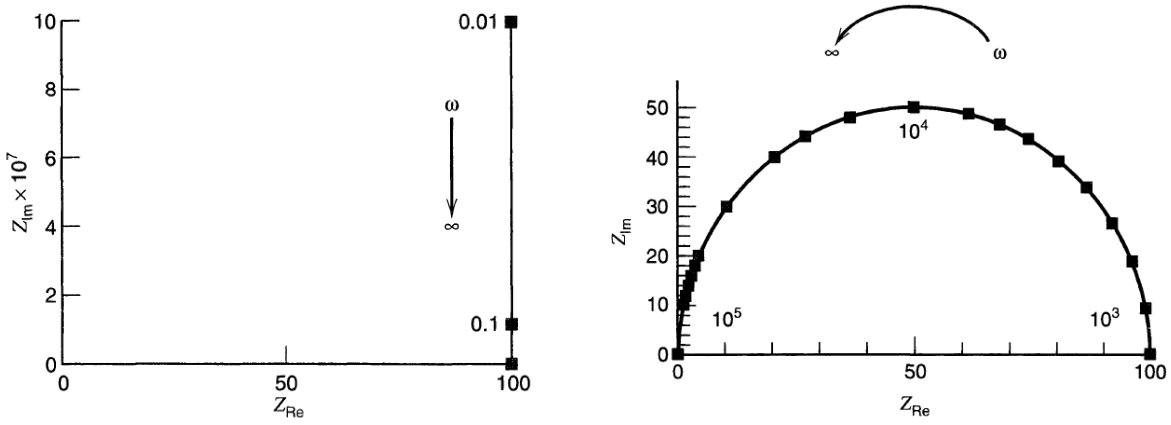

(a) Series RC circuit

(b) Parallel RC circuit

Figure 2.6: Nyquist plot of a RC circuit in a) series and b) parallel, with $R = 100\Omega$ and $C = 1\mu F$ [6]

If an electrochemical interface is examined, one can describe this by a Randles cell as shown in Figure 2.7a [12] [66]. This circuit describes the charge transfer through the interface layer.

According to Brett [12], in a practical sensing situations, the Nyquist plots do not usually afford perfect semicircles as the one in Figure 2.7a. In this practical sensing situation, the semicircles can be ”depressed” and the expected vertical straight lines near the x-axis become less than $90°$, as shown in Figure 2.7b. This phenomenon can be attributed to surface non-uniformity and roughness, and porosity, in that each local sub-microscopic area gives rise to its own RC combination. However, what is observed is the macroscopical sum of all these contributions. Often, this is described as frequency dispersion and can be seen as the constant phase element (CPE) as described in Equation 2.34 [12].

From a Nyquist plot with a semi-circle, the resistance and capacitance of this RC circuit semi-circle can be determined. The resistance of a semi-circle can be found at the x-axis. The horizontal distance

between the start and end of the semi-circle is the resistance of the RC circuit. The capacitance of this RC circuit can be found by using the equation of Equation 2.39 [12].

$$C = \frac{1}{R\omega_{\text{max}}} \tag{2.39}$$

Here, C is the capacitance, R is the resistance of the semi-circle and ω_{max} is the maximum frequency on top of the semi-circle.

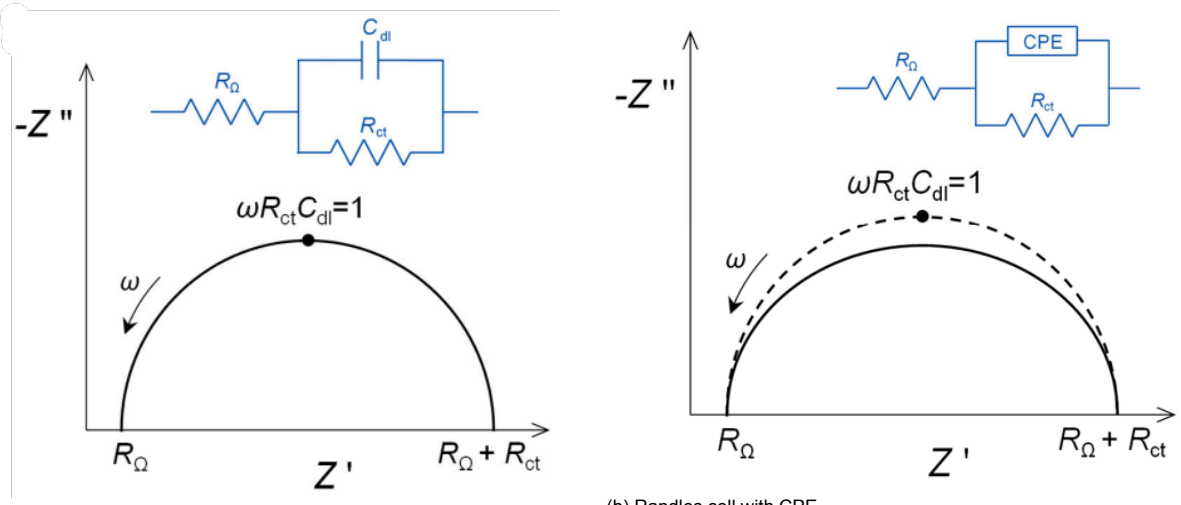

(a) Randles cell

(b) Randles cell with CPE

Figure 2.7: Nyquist plot of a) Randles Cell and b) Randles Cell with CPE [12]

2.4.2. Monopolar membranes

Monopolar membranes are ion-exchange membranes that are charge selective and therefore only transport cations or anions, as discussed in section 2.2. Anion and cation exchange membranes can be examined using EIS and will have the same equivalent circuit.

According to many literature studies, the equivalent circuit of a monopolar membrane would consist of two Randles cells in series. These two Randles cells distinguish the diffusion boundary layer (DBL) and the double layer (DL) [60] [56] [90].

However, according to Gurreri et al. [40], Długołęcki et al. [23], Kozmai et al. [45] and Zhao et al. [91], at low salt concentrations (0.017M NaCl) the dominant resistance is the DBL resistance, whilst the contribution of the pure membrane resistance and DL resistance are minimal. At higher salt concentrations (equal or higher than 0.5M NaCl, as used in this research), the dominant resistance is the pure membrane resistance, the DBL plays a considerable role and the DL is insignificant [40].

Therefore, the equivalent circuit of Figure 2.8 is used for monopolar membranes with salt concentrations of 0.5 M NaCl and higher. Other equivalent circuits can be considered, but this is further explained in Appendix B.

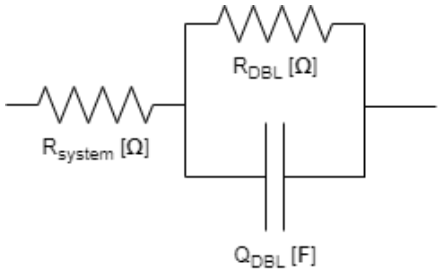

Figure 2.8: Equivalent circuit of a monopolar exchange membrane

2.4.3. Bipolar membranes

The electrical equivalent circuit of a bipolar membrane (BPM) is examined by Blommaert et al. [9] and different from monopolar membranes. This difference is mostly induced by the presence of the water dissociation reaction inside the BPM (under reverse bias). Figure 2.9a shows a bipolar membrane (BPM) in an electrochemical cell with corresponding chemical reactions. Figure 2.9b, describes a corresponding equivalent circuit of the BPM in Figure 2.9a.

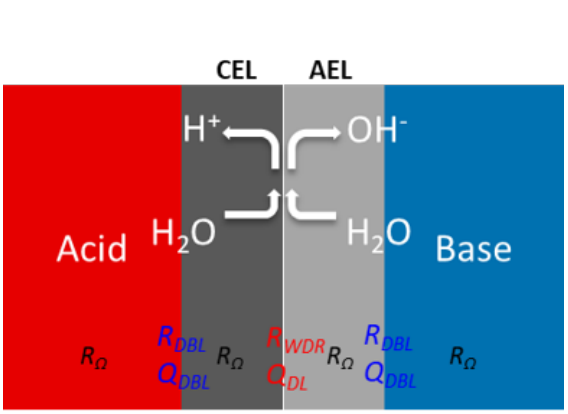

(a) BPM reactions

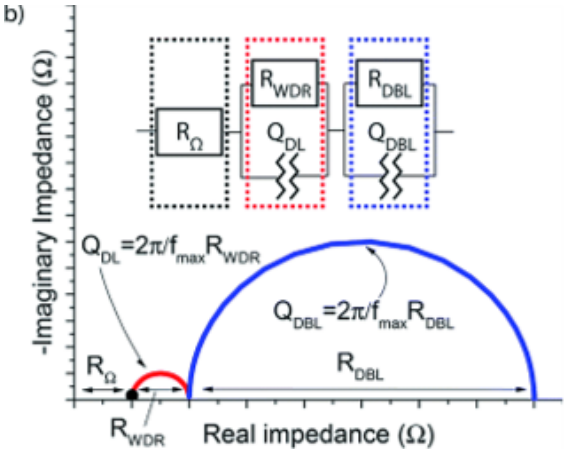

(b) BPM EIS Nyquist plot [9]

Figure 2.9: BPM reactions and corresponding EIS plot under reverse bias

Figure 2.10 shows the equivalent circuit of a BPM as also presented in Figure 2.9b. This circuit can be divided in to three parts, where the first part, R_Ω, is related to the ohmic resistance of the combined membrane layers. Since this component follows Ohm's law ($V = IR$), and there is no capacitive effect in R_Ω, it is independent of frequency. The resistance R_Ω can be determined from a Nyquist plot by measuring the distance between the origin and the start of the first semicircle. This resistance includes the ohmic resistance of the membrane and the ohmic resistance of the solutions from the membrane to the reference electrodes [9].

Hereafter, the second part of the circuit describes the water dissociation reaction (WDR) as a resistance (R_{WDR}) and a non-ideal capacitor (Q_{DL}), also called a Constant Phase Element (CPE) [9]. This part can be observed as the first semi-circle in the Nyquist plot. The horizontal axis represents the ohmic resistance (R_{WDR}), whilst the vertical axis represents the non-ohmic part (Q_{DL}).

Finally, the third part shows the resistance (R_{DBL}) and CPE (Q_{DBL}) of the diffusion boundary layer of the membrane, and can be found as the second semi-circle in the Nyquist plot. The horizontal axis represents the ohmic resistance (R_{DBL}), whilst the vertical axis represents the non-ohmic part (Q_{DBL}).

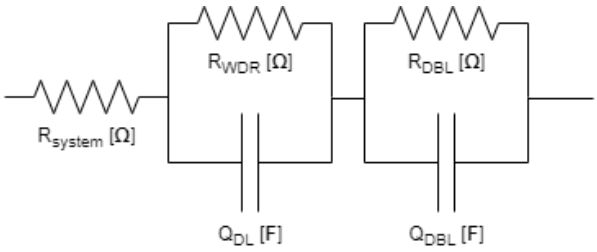

Figure 2.10: Equivalent circuit BPM

2.4.4. Membranes in series

In the past, EIS has been used in several flow battery studies [9][76][60][23]. Most of the recent literature studies are focused on only single parts of flow batteries. However, Trovò et al. [76] uses a 40-cell stack of a vanadium redox flow battery, where a 40-cell stack is examined with many membranes in series.

For the ABFB, the equivalent circuit of a whole triplet is depicted in Figure 2.11. Here, an anion exchange membrane, bipolar membrane and cation exchange membrane are placed in series, divided by different aqueous solutions.

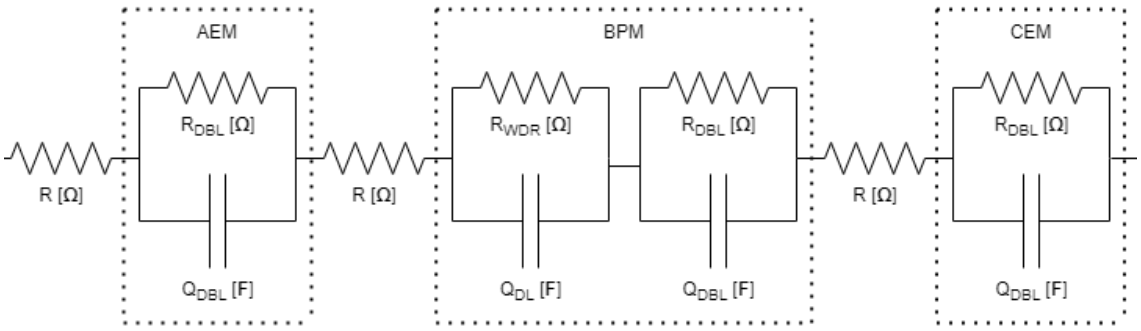

Figure 2.11: Equivalent circuit of a whole AEM, BPM, CEM triplet

3

Methodology

In this chapter, the methodology is explained. Section 3.1, presents the approach of the experiments, whereafter section 3.2 shows the experimental setup including the used components. In section 3.3, the design, manufacturing and testing process of a flowframe stack is shown. Section 3.5, will elaborate on the potentiostat and finally, in section 3.6 the data processing will be clarified.

3.1. Approach

To analyse the non-ohmic resistance of multiple ion-exchange membranes in series, stated as the aim of this research, a variety of experiments have been carried out. To measure the non-ohmic resistance of the membranes, Electrochemical Impedance Spectroscopy (EIS) is used (this method is explained in section 2.4).

To answer the first sub-question of this research as stated in chapter 1, the effect of different current densities on the ohmic and non-ohmic resistance of a bipolar membrane (BPM) under forward and reverse bias has to be observed.

To find out if it is possible to compose a simplified equivalent circuit of multiple ion-exchange membranes in series by using EIS data (as stated in the second sub-question in chapter 1), all three single membranes of the triplet are examined as a starting point. Thereafter, a full stack of three membranes (AEM, BPM and CEM) in series is analysed.

3.2. Stack setup

In this section, the experimental setup is explained. First, the cell configuration for the current density measurements is shown in subsection 3.2.1. Hereafter, the used membranes are shown in subsection 3.2.2.

3.2.1. Six-compartment setup

The six-compartment setup is used for experiments to analyse the impact of different current densities on the non-ohmic resistance of BPMs. The rest of the experiments are executed with the Flowframe stack as explained in more detail in section 3.3.

The six-compartment setup of Figure 3.1a has 100 ml compartments for electrolyte (Na_2SO_4), salt (NaCl), acid (HCl) and base (NaOH). At both sides of the BPM, a luggin capillary is placed, directing the reference electrodes to the membrane (see schematic overview of Figure 3.1b). These luggin capillaries are connected to 8 mm leak-free Ag/AgCl reference electrodes.

To induce an ion-flow and let a water association or dissociation reaction take place inside the BPM, a working electrode and counter electrode are applying a potential to the setup. This water dissociation or water association reaction as well as the diffusion boundary layer, is measured by the reference electrode.

Due to the reference electrode (RE) next to the BPM membrane, this setup only measures over the BPM in the centre of the setup. The other compartments, working and counter electrode make sure

the reaction inside the BPM can take place.

During the experiments with this setup, the pumps are switched off and therefore provide no flow, to avoid noise in the measurements during the experiments. However, before every experiment the compartments are drained and refilled to make sure the concentrations of the solutions stay equal over multiple measurements.

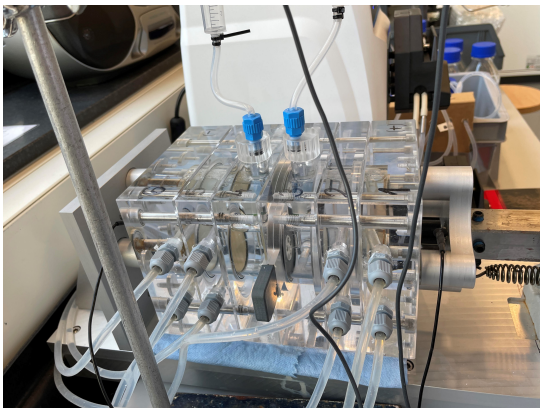

(a) Six-compartment setup

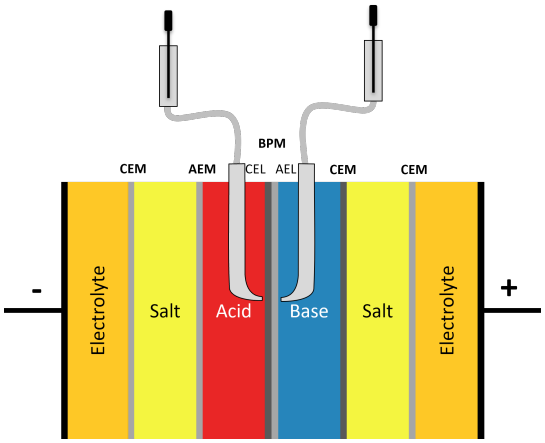

(b) Schematic overview

Figure 3.1: Six-compartment setup at Delft University of Technology and schematic overview six-compartment setup with luggin capillary and reference electrodes

3.2.2. Membranes

For all experiments, Fumatech ion-exchange membranes are used as shown in Table 3.1. For the anion exchange membranes (AEM), the fumasep® FAB-PK-75 membranes are used. For the bipolar membranes (BPM), the fumasep® FBM-PK membranes are used. For the cation exchange membranes (CEM), the fumasep® FKB-PK-75 membranes are used [36].

The membranes are made of polyetheretherketone (PEEK), which is an aromatic polyether, high-performance thermoplastic used in coating, insulation of high-performance wire and cable, and molded parts [25]. In this case, PEEK is used as reinforcement of the main composite material, because it is resistant to solvents.

Table 3.1: Ion-exchange membranes used for experiments

Membrane	Type
AEM	fumasep® FAB-PK-75
BPM	fumasep® FBM-PK
CEM	fumasep® FKB-PK-75

3.3. Flowframe stack design, manufacturing and testing

A stack with thin flowframes is required to measure multiple membranes in series, with the possibility to measure every membrane individually as well. A stack with these specific requirements is not available and therefore is designed, manufactured and tested.

3.3.1. Flowframe stack design

The stack is designed in Autodesk Fusion 360 and based on a previous design for a stack using spacers. The flowframes are designed to be as thin as possible to avoid having an interference of the resistance of the solutions on the results. However, to have the possibility to put reference electrodes in every compartment close to the membrane, there has to be a hole in the flowframes for 1.0 mm reference electrodes. Therefore, the designed flowframes of Figure 3.2 are 3.0 mm thick with a 1.0 mm wide tunnel to the 22 cm^2 membrane area. This allows a 1.0 mm reference electrode to enter the flowframe

and the flowframe to preserve its strength. In this design, three different flowframes are produced: an acid flowframe as depicted in Figure 3.2a, and a base and a salt flowframe with a different configuration. The end-plates of the stack contain the working and counter electrode, including the compartment for the electrolyte.

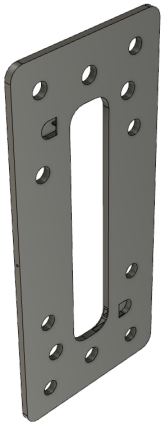

(a) Acid flowframe

(b) Triplet flowframes

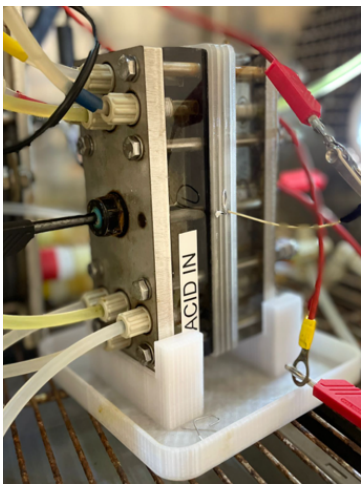

(c) Final stack

Figure 3.2: CAD design of multiple 3.0 mm thick flowframes with a membrane area of 22 cm^2 and the final stack

3.3.2. Flowframe stack manufacturing

The manufacturing process is done by a filament 3D-printer, using PETG as filament. PETG is chosen because of its manufacturability as well as chemical resistance over time. To obtain a leak-free stack, five aspects are important during the printing process.

First, the printing surface needs to be as flat as possible. Using a glass bed is recommended, because a coated spring steel bed has a higher roughness level.

Second, in the settings of the 3D printing model the infill of the 3D print has to be 100%. Otherwise, the flowframe is partly hollow and the aqueous solutions could move easier into the material if an imperfection is present in the print.

Third, the printing resolution has to be as high as possible. The highest resolution of the used 3D printer was 0.1mm per layer. This resolution was required, because of the chance of imperfections during the print. If a 3D printer uses a higher layer thickness, the print can become porous. Which could induce leakages under high pressure of the aqueous solutions. To avoid this phenomenon, thinner layers are recommended.

Fourth, to be able to use reference electrodes inside the stack, holes for the reference electrodes have to be present. In the 3D print design, a 1.0 mm hole is present, providing a channel for the reference electrode. Because this hole will be constructed layer by layer, in horizontal direction, this hole could collapse during the printing process. Therefore, the hole is printed in the water drop shape of Figure 3.3. This water drop shape prevents the channel to collapse during the printing and assembling process.

Finally, the top surface has to be ironed. The ironing process will smooth out the top surface and makes sure there are no pits in the surface that could cause leakage.

After the prints are finished, the reference electrode holes are drilled with a 1.0 mm drill. To make sure the surface is smooth enough, the surface is sanded with fine (360 grit or higher) sandpaper. For the reference electrodes, two leak-free 1.0 mm LF-1.0-100 Innovative Instrument reference electrodes are used. The unused holes in the flowframes are filled with plugs during operation.

A 0.5 mm EPMD rubber gasket is used as a seal, because of its chemical resistance properties [33]. The plate rubber is die-cut into the shape of the gasket. To make sure the stack is leak tight, a few points have to be taken into account. To obtain a sufficient seal, a flat surface is used for this stack.

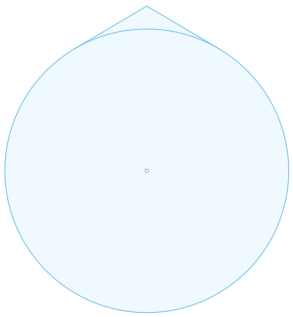

Figure 3.3: Hole for a 1.0 mm reference electrode, in water drop shape at the 3D print.

For a fully sealed membrane and flowframes, two gaskets are used in between two flowframes. That means that in this stack, a gasket-membrane-gasket setup is used between two flowframes.

The used membranes as stated in Table 3.1, are prepared by a die-cut in the right shape and stored in a 0.25 M NaCl solution.

Whilst assembling the stack, the sequence of Figure 3.4b is used. The stack has an extra salt flowframe to be able to measure over the three membranes. This makes it possible to measure a whole triplet, from salt to salt, by reference electrodes.

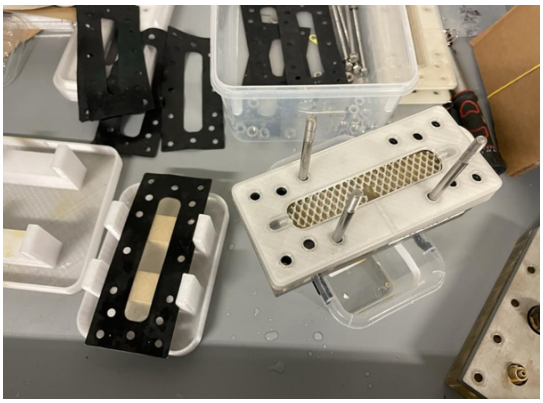

(a) Assembling process of the flowframe stack

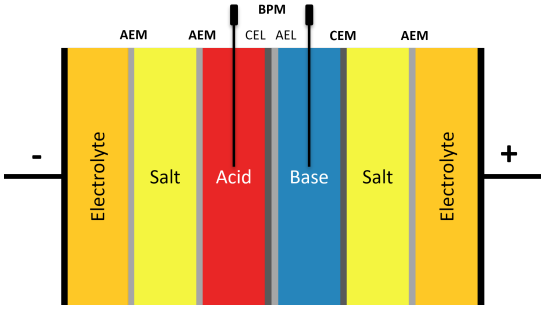

(b) Schematic overview flowframe stack

Figure 3.4: Assembling process flowframe stack and schematic overview flowframe stack with reference electrodes

Between two flowframes, a gasket, membrane and second gasket are placed. This assembling process is shown in Figure 3.4a. In the flowframes a mesh (with a hole for the reference electrode) is placed to make sure the solution is mixed inside the compartment [78]. For a proper gasket seal, compression of the gaskets has to be around 40% [29]. To obtain this compression rate, Equation 3.1 is used to calculate the stiffness k by giving the input of the elastic modulus of EPMD ($E = 6.73MPa$ according to [92]), the area of the gasket ($A = 9550mm^2$) and the thickness of the 10 gaskets in series ($L = 0.5 * 10 = 5mm$). In this equation the stiffness of the gaskets is calculated, but the stiffness of the end-plates, flowframes and membranes are neglected.

$$k = \frac{E * A}{L} = 12.85 \frac{kN}{mm} \tag{3.1}$$

The stiffness of the ten used gaskets is equal to $k_{\text{gaskets}} = 12.85 \frac{kN}{mm}$. The axial force on the stack can be calculated by Equation 3.2, with a compression of $Comp = 0.40$, and the total length of compression is $L = 5mm$.

$$F_{\text{axial, total}} = Comp * k_{\text{gaskets}} * L \tag{3.2}$$

The total axial force on the stack has to be $F_{\text{axial, total}} = 25.7kN$, divided by eight bolts makes an axial force of $F_{\text{axial, one bolt}} = 3.2kN$ per bolt. To obtain this force by the bolts, they have to be tightened until a certain torque. This torque can be calculated using Equation 3.3, with a bolt diameter of $d_{\text{bolt}} = 6mm$ (in case of a M6 bolt) and a torque coefficient of $K = 0.2$ [52] [48].

$$T = F_{\text{axial, one bolt}} * K * d_{\text{bolt}} \tag{3.3}$$

For this stack to obtain a total gasket sealing, it requires a compression rate of 40%. This compression can be achieved by applying a torque of $T = 3.85Nm$ to the eight M6 bolts.

3.3.3. Flowframe stack testing

To be sure that the stack works as required, it is essential to test the stack. The stack testing follows three steps.

First, the stack is connected to the pumps and filled with demineralised water and the pumps are switched on. A visual inspection makes sure there is no external leakage.

Second, an internal leakage test is executed. To perform an internal leakage test, all compartments are filled with demineralised water water. All (top) outlets are disconnected and left open, except from one flowframe. Turn on the flow in the connected flowframe and watch if the other compartments do not leak at the top outlet. Repeat this method for all compartments.

Third, conduct an IV-curve and check if the curve of the plot is as expected from literature [84]. An IV-curve is a plot showing the voltage response of the stack under different currents. If no current is applied ($I = 0A$), the open circuit voltage (OCV) can be measured. If a positive current is applied, the battery will be charged and the voltage increases compared to the OCV. In case a negative current is applied, the battery will discharge and the voltage response will decrease compared to the OCV. For the flowframe stack, the IV-curve of Figure 3.5 is conducted.

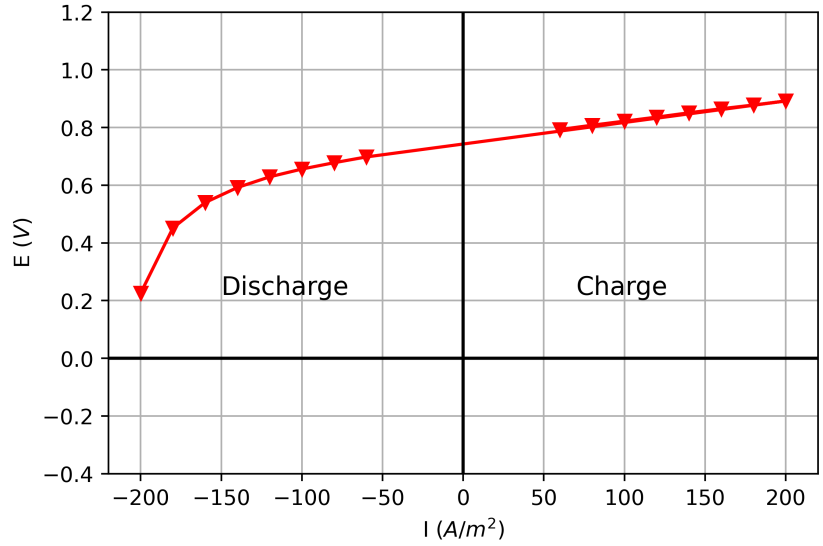

Figure 3.5: IV-curve of the flowframe stack, using the chemical compounds of Table 3.2

In Figure 3.5, the open circuit voltage (OCV) at $I = 0A/m^2$ is with $E_{\text{OCV}} = 0.76V$ lower than the expected OCV of $E_{\text{OCV}} = 0.864V$, from the calculation of Equation 2.24. This can be explained by a few factors, if the standing time is too brief, the voltage does not fully recover (no equilibrium) and no real OCV can be measured. Also, the State of Charge (SOC) can be lower than anticipated. If the concentrations of the solutions are different than used for the calculations, the measured OCV is not what you would expect [86]. Finally, a broken membrane, different temperatures a gasket leak and/or membrane impurities can influence the OCV measurement [86] [89].

A more rapid decrease in voltage response can be found for currents lower than $-150A/m^2$. According to internal research of AquaBattery [84], this phenomenon appears if there is a background concentrations of (more than 0.01M NaCl) salt present in the acid and base solutions. Since the membranes are stored in salt solutions, and although the system and the membranes are flushed with demineralised water, it can be expected that a very small amount of salt still is present. This explains the IV-curve of Figure 3.5.

3.4. Experiments

The solutions of Table 3.2 are used to conduct the experiments. A different electrolyte is used in the six-compartment setup and therefore, CEM membranes are used between the electrolyte and salt compartments instead of AEM. For the flowframe stack, AEM membranes are used between the electrolyte and salt compartments, to let Cl^- ions pass.

Table 3.2: Chemical compounds and concentrations for an acid-base flow battery

Solution	Concentration [M]	Chemical compound	Conductivity $[mS/cm]$	Resistance $[\Omega/mm]$
Salt	0.5	NaCl	41	0.11
Acid	1.0	HCl	318	0.014
Base	1.0	NaOH	178	0.026
Electrolyte flowframe stack	0.25	Fe(II)Cl	-	-
	0.25	Fe(III)Cl	-	-
	0.1	HCl	-	-
Electrolyte six compartment	1.0	Na_2SO_4	-	-

For EIS measurements in the flowframe setup, the 1.0 mm reference electrodes are used. Single membrane measurements are done by placing the reference electrodes in the flowframes next to the membrane of measurement. To conduct the triplet measurements, the reference electrodes are placed in both salt compartments, shown in Figure 3.4b. In this way, a whole triplet can be measured including the AEM, BPM and CEM and solutions.
The conductivity and resistance of the solutions can be determined. In Figure 3.6, the conductivity of the acid, base and salt solutions under different concentrations are shown [85].
From these figures, the conductivity of the fluids can be obtained. The corresponding resistance can be calculated using Equation 3.4.

$$R = \frac{L}{k * A} \tag{3.4}$$

Here, the resistance of the fluids is calculated with the conductivity k, length of the fluids per millimeter $L = 1mm$ and area of the membrane A. For the flowframe stack, the membrane area is $A = 2200mm^2$, the concentration for acid and base are 1 M and the concentration of salt is 0.5 M, which concludes to a resistance in $[\Omega/mm]$ as shown in Table 3.2.

During the flowframe stack measurements, the flow of the solutions is set at $40ml/min$. This flow rate can be converted to an average rate of the fluid in cm/s, parallel to the membrane in vertical direction by Equation 3.5.

$$1[ml/min] = \frac{1}{60 * area[cm]}[cm/s] \tag{3.5}$$

For a flow rate of $40ml/min$, this means that the solutions pass the membrane at $1.11cm/2$.

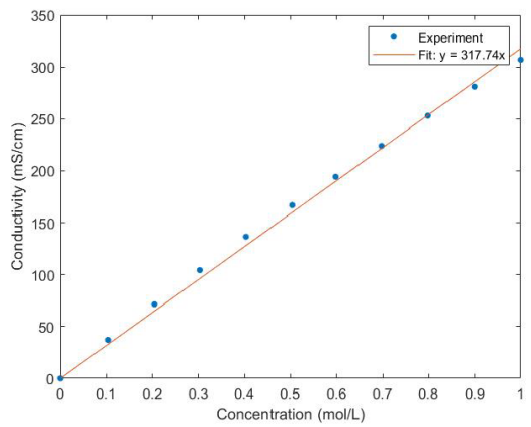

(a) Acid (HCl)

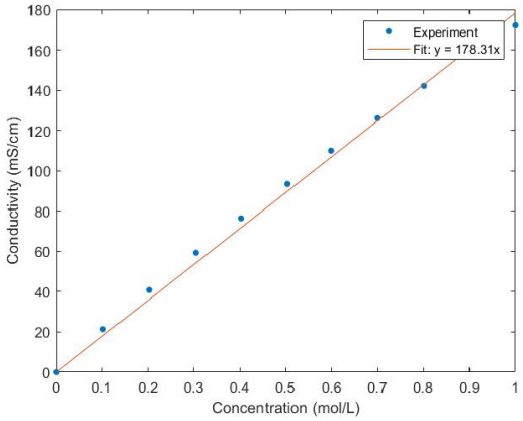

(b) Base (NaOH)

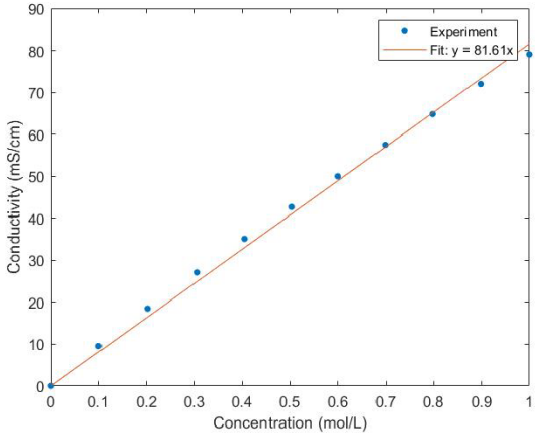

(c) Salt (NaCl)

Figure 3.6: Conductivity of acid, base and salt, as a function of the concentrations of the fluid streams including fits. [85]

3.5. Potentiostat

For electrochemical impedance spectroscopy (EIS), a potentiostat is required. A potentiostat is an electronic instrument that controls the voltage between a working electrode and a reference electrode [38]. For this research, the potentiostat is used in galvanostatic mode. In galvanostatic mode, the instrument will control the current instead of the voltage. This is necessary for controlling the electrochemical reaction inside the BPM. By controlling the current, the ion flow can be controlled and therefore, the electrochemical reaction inside the BPM can be controlled.

Two reference electrodes are used for EIS of ion-exchange membranes in an acid-base flow battery: one sensing electrode and one reference electrode. The sensing electrode measures the phase and voltage before the membrane and the reference electrode will measure the phase shift and voltage after the membrane.

Figure 3.7 shows how the potentiostat is connected to the stack. The sensing electrode (S) is connected to the compartment on the side of the working electrode and the reference electrode is connected to the compartment on the side of the counter electrode.

Two different potentiostats are used for the experiments. The current density measurements are done by the AUTOLAB PGSTAT302N at the Delft University of Technology. The operational instructions are described in Appendix C.

For the rest of the experiments, the IVIUM-N-STAT is used at AquaBattery. The software is different, but the working principle is equal to the AUTOLAB potentiostat.

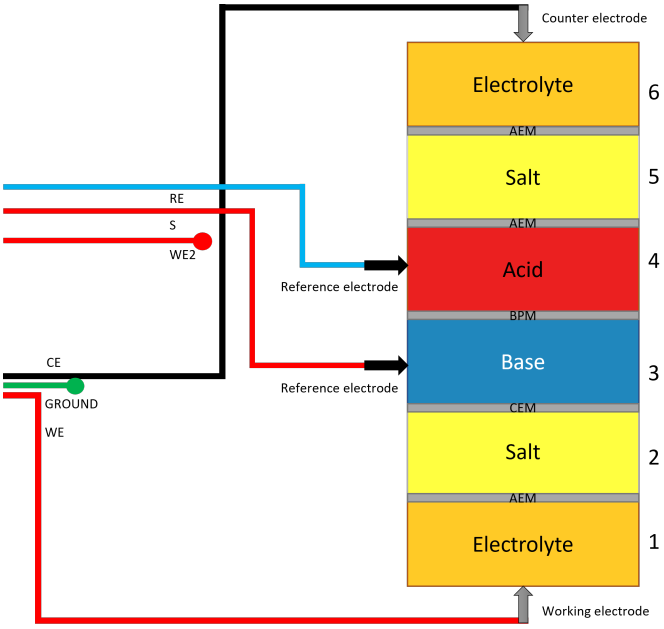

Figure 3.7: Schematic overview of connecting the potentiostat to the stack

3.6. Data processing

For this research, the Python code in Appendix A is developed and written. This code is used to process the EIS data because this code was easier to use for different potentiostat outputs than other, commonly used software. This Python code is able to process the Excel file output of the potentiostats and provide figures in the same style, independent from which potentiostat is used. Another benefit of using Python is that the data can easily be processed in other ways as well. New calculations, proper comparisons and clarifying graphs can easily be obtained.

To construct proper Nyquist and Bode plots with multiple measurements plotted in one figure, multiple Python packages are used.

For the construction of dataframes, pandas [58] is used. Pandas can read Excel files and produce structured dataframes, which can be used to conduct clear graphs and equations. The plotting of Nyquist and Bode plots is done by Matplotlib [50], because Matplotlib can construct multiple plots in one figure, which is necessary for this research. The EIS fitting is done using the ImpedancePy package [42], because this software can make fits for EIS dataframes and provide the (non-)ohmic values of these fits.

4

Results and Discussion

In this chapter, the results of the different experiments are shown and discussed. In section 4.1, the results are presented of the bipolar membrane (BPM), during water association and dissociation with varying background currents. In section 4.2, the flow rate is varied to analyse the effect of the flow rate on the boundary layers. Electrochemical impedance spectroscopy is applied on single membranes in section 4.3, whilst in section 4.4 the membranes in series are analysed. Finally in section 4.5, a simplified equivalent circuit is constructed.

4.1. Current densities

In this section, varying current densities are applied to the bipolar membrane (BPM) in the six-compartment setup of Figure 3.1a.

If a positive current is applied to the setup, water will be dissociated inside the BPM to form H^+ and OH^- ions. Water dissociation takes place during charging the battery and is also called reverse bias [63]. For the rest of this report, this will be called water dissociation.

Applying a negative current to the stack, induces the association of H^+ and OH^- ions into water inside the BPM [63]. This reaction occurs when the battery is discharged an is also called forward bias. For the rest of this report, this will be called water association.

In Figure 4.1, water association takes place inside a BPM under different background currents. In Figure 4.2, water is dissociated inside the BPM under different background currents.

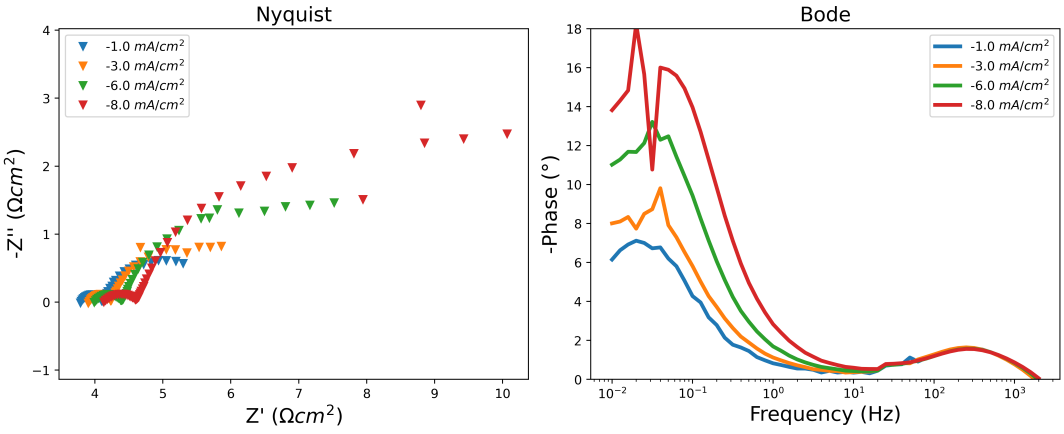

Figure 4.1: EIS of water association inside a BPM under different background currents (forward bias)

According to Blommaert et al. [9], in Figure 2.9, the first semi-circle is caused by the water association reaction, whilst the second semi-circle is caused by the diffusion boundary layer. The offset of the plots

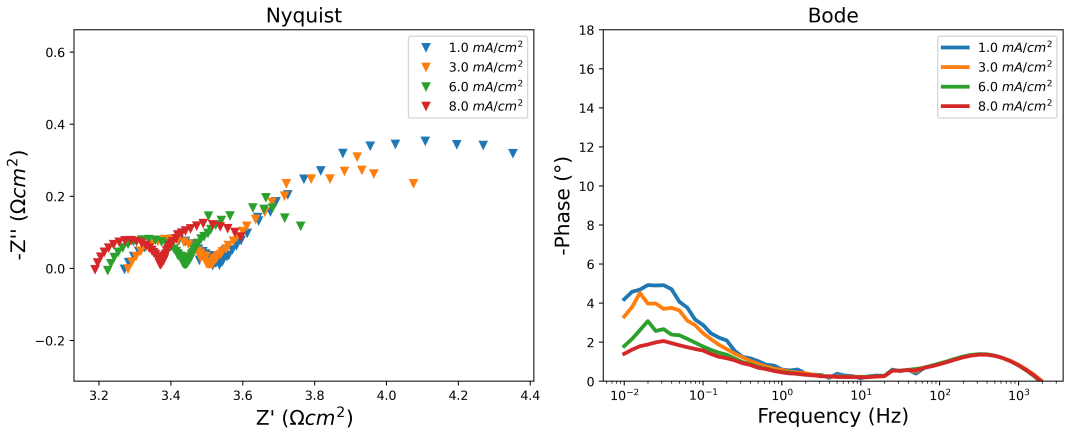

Figure 4.2: EIS of water dissociation inside a BPM under different background currents (reverse bias)

Table 4.1: Resistances of BPM with varying background currents, as shown in Figure 4.1 and Figure 4.2

Background current [mA/cm^2]	R_{system} [Ω cm^2]	R_{WDR} [Ω cm^2]	Q_{DL} [F cm^2]	n_{DL}	R_{DBL} [Ω cm^2]	Q_{DBL} [F cm^2]	n_{DBL}	R_{Total} [Ω cm^2]
8.0	3.19	0.188	0.00748	0.872	0.246	19.6	-	3.624
6.0	3.24	0.197	0.00466	0.933	0.487	10.1	0.745	3.924
3.0	3.30	0.207	0.00559	0.899	0.912	5.31	0.681	4.419
1.0	3.28	0.26	0.0129	0.771	1.03	4.59	0.789	4.57
-1.0	3.81	0.302	0.00618	0.866	1.69	3.28	0.806	5.802
-3.0	3.93	0.307	0.00577	0.874	2.26	2.51	0.818	6.497
-6.0	4.03	0.374	0.00689	0.824	4.1	1.28	0.804	8.504
-8.0	4.19	0.43	0.00615	0.822	7.09	0.679	0.787	11.71

are caused by the ohmic resistance of the system. The x-axis represents the ohmic resistance, whilst the y-axis represents the non-ohmic resistance.

In the Bode plots of Figure 4.1 and Figure 4.2, two peaks can be found. One peak can be found around 200Hz, corresponding to the diffusion boundary layer. The second peak can be found around 0.03Hz and corresponding to the water association reaction. During water association, the second semi-circles of the Nyquist plot are large compared to the second semi-circles of the water dissociation plot. However, in both plots the reaction takes place at the same frequencies.

In Table 4.1, the varying resistances as a function of the background current are presented and the total ohmic resistance is shown in the last column. The resistance of the first semi-circle is expressed as R_{WDR} and the resistance of the second semi-circle is shown as R_{DBL}. The non-ideal capacitors or constant phase elements (CPE) are depicted as Q_{DL} and Q_{DBL}. The n_{DL} and n_{DBL} stand for the fitting parameter n, as stated in section 2.4 and Equation 2.34.

The shape of the first semi-circle is similar during water association and dissociation, but if the relative background current decreases, the resistance of the water reaction inside the BPM increases. According to Tanaka [73], this increase in resistance has to do with the decreasing ion concentration and therefore, a decrease in conductivity.

For the BPM with water association in Figure 4.1, the second semi-circle (diffusion boundary layer), is causing a large part of the ohmic and non-ohmic resistance. When the background current becomes more negative, the diffusion boundary layer resistance contributes more to the (non-)ohmic resistance.

For the BPM with water dissociation (Figure 4.2), with higher background currents, the second semi-circle is contributing less and the total resistance decreased as a function of background current.

The total resistance of the EIS measurements under different current densities, is plotted as a function of the background current in Figure 4.3.

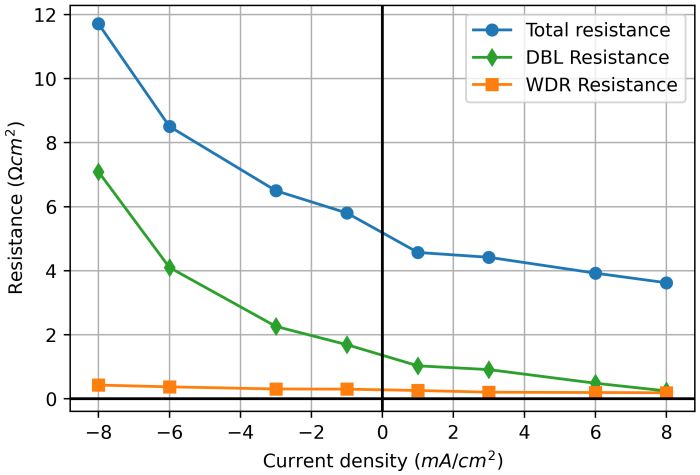

Figure 4.3: BPM resistance as function of the current density

In Figure 4.3, the total resistance, DBL resistance and WDR resistance of the BPM are shown under different current densities, based on the data of Table 4.1. The total resistance is the sum of the DBL resistance, WDR resistance and the ohmic resistance of the BPM.

The WDR resistance becomes linearly smaller over the current density. This could be caused by the increasing concentration of H^+ and OH^- ions inside the BPM under higher current densities. The higher concentrations of acid and base are more conductive, as shown in Figure 3.6 [85]. When H^+ and OH^- ions recombine, H_2O is formed inside the BPM and this will contribute to a lower concentration.

In this visualisation, it becomes clear that the DBL resistance has an exponential decline with respect to the current density. An approximation of the DBL resistance in this figure can be found in Equation 4.1.

$$R_{\text{DBL}} = 1.37 * e^{-0.195*I} \tag{4.1}$$

In this equation, R_{DBL} is the DBL resistance and I is the applied current density in $[mA/cm^2]$. The equation of Equation 4.1 is not a general equation for all setups and settings, but it gives an indication of the course of the graph with the given stack and parameters.

The hypothesis for the phenomenon of resistance shifting under different background current, is that due to water association (Figure 4.1), the boundary layer is getting depleted of ions, by the absorption of H^+ and OH^- ions into the BPM. This is illustrated in Figure 4.4a.

For water dissociation (Figure 4.2), the hypothesis is the other way around. The diffusion boundary layer is getting enriched by ions, due to the release of ions by the BPM. This could make the DBL more conductive, which leads to a lower resistance. This hypothesis is illustrated in Figure 4.4b.

The decreasing WDR resistance seems to have the same development as Długołecki et al. [23] states with the graph of Figure 4.5. Długołecki et al. shows that the resistance of the DBL of cation exchange membrane decreases as a function of the flow rate. The flow mixes the DBL, what could make the DBL more conductive in case ions are pulled inside the membrane and the DBL gets depleted. However, this is only measured for an AEM and CEM and not for a BPM between the same solutions as the BPM of Figure 4.3.

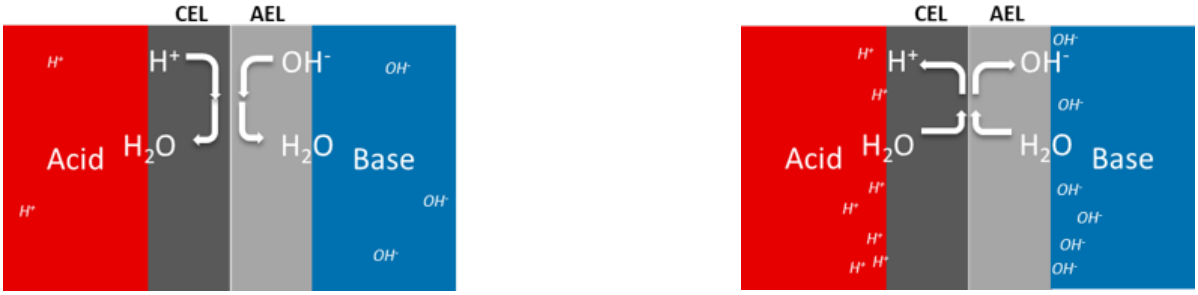

(a) Depletion during water association (forward bias)

(b) Enrichment during water dissociation (reverse bias)

Figure 4.4: Hypothesis depletion and enrichment of the BPM diffusion boundary layer

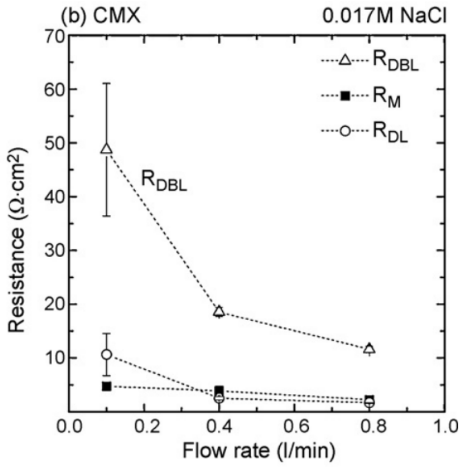

Figure 4.5: Resistance of a CEM, with membrane resistance R_M, double layer resistance R_{DL} and diffusion boundary layer resistance R_{DBL} in a 0.017 M NaCl solution [23]

4.2. Flow rate difference

The hypothesis for the phenomenon of resistance shifting under different background currents as stated in section 4.1, is that due to water association (Figure 4.1), the boundary layer is getting depleted of ions, by the absorption of H^+ and OH^- ions into the BPM (as shown in Figure 4.4).

To test this hypothesis, in this section the (non-)ohmic resistance of the diffusion boundary layer is measured at different flow rates. Previous research shows that the DBL resistance reduces when the velocity of the feed water increases, since the mixing rate will be improved at higher velocities [79] [81] [22] [24] [23] [60]. Higher flow rates, may refresh the boundary layer faster and this might be detectable in the non-ohmic resistance part of the BPM boundary layer.

Since the experiments of section 4.1 were executed in Delft, and the test setup at Delft University of Technology (Figure 3.1a) has large compartments without any flow, the flow experiments are executed at the flowframe setup of Figure 3.2b. Because these experiments are executed at another location, with another potentiostat, a comparison of the different potentiostats is made in subsection 4.2.1.

In subsection 4.2.2, the flow rate experiments are explained and the results are shown.

4.2.1. IVIUM & AUTOLAB comparison

To check if IVIUM potentiostat/galvanostat results are comparable with the AUTOLAB potentiostat/galvanostat, an experiment has been executed using the flowframe setup at both the IVIUM at AquaBattery and the AUTOLAB at Delft University of Technology. In Figure 4.6a and Figure 4.6b, the same flowframe setup has been used, with equal flow rates (54 ml/min) and background currents (-6.0 mA/cm^2), to measurements with the IVIUM and the AUTOLAB potentiostat.

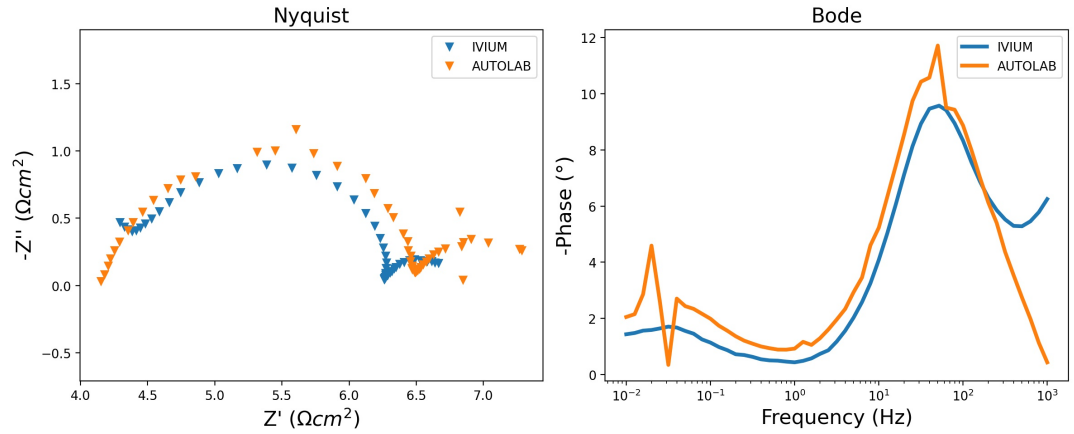

(a) -6.0 mA/cm^2 (water association)

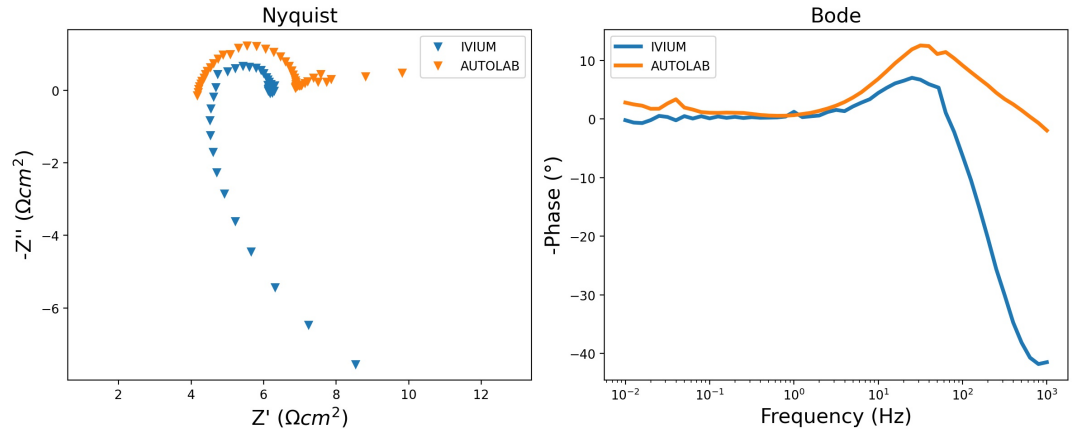

(b) 6.0 mA/cm^2 (water dissociation)

Figure 4.6: EIS of the IVIUM vs AUTOLAB potentiostat

A few differences between the IVIUM and the AUTOLAB can be observed. First, in Figure 4.2, a long tail is present in the Nyquist plot at the higher frequencies of IVIUM. This tail does not show at the AUTOLAB measurements. This artifact can be caused by different interfering signals at the different labs. Also, the IVIUM shows a smaller first semi-circle, for the water association/dissociation reaction. However, the plots have the same shape and behaviour in the range of 10^{-2} < Hz < 300. Finally, less noise is observed in the IVIUM measurements. For the setup for the IVIUM measurements, longer tubes were used between the pump and the stack compared to the AUTOLAB measurements. This could have a dampening effect to the pump pulsation and could lead to less noise during the measurements.

4.2.2. Flow rate measurements

To measure the effect of flow rate on the second semi-circle in a Nyquist plot of a bipolar membrane (BPM), multiple EIS experiments are done on the flowframe test setup. Because the second semi-circle of the BPM was the largest and therefore most noticeable at a background current of $-8.0 mA/cm^2$ (see Figure 4.1 and Table 4.1), this background current is chosen for the flow rate measurements.
To determine the effect of flow rate, the flow rate is converted from ml/min to cm/s as shown in Equation 3.5. This is the rate of the fluid, parallel to the membrane in vertical direction. This flow rate gives a more representative number for the flow through the flowframe, parallel to the membrane.
According to Vermaas et al. [80], the refreshing of the layers adjacent to the membrane scales with the Reynolds number, with respect to the flow parallel to the membrane. The Reynolds number Re can be calculated using Equation 4.2 [80] [70].

$$Re = \frac{v d_h \rho}{\mu} \tag{4.2}$$

Table 4.2: Resistances of BPM with varying flow rates, as shown in Figure 4.7

Flow rate [cm/s]	Re	R_{system} [Ω cm^2]	R_{WDR} [Ω cm^2]	Q_{DL} [F cm^2]	n_{DL}	R_{DBL} [Ω cm^2]	Q_{DBL} [F cm^2]	n_{DBL}	R_{Total} [Ω cm^2]
0	0	4.57	1.43	0.00294	1	0.56	9.43	1	6.56
0.14	7.6	4.79	1.3	0.0033	1	0.203	38	1	6.293
1.11	61	4.58	1.35	0.003	1	0.181	63.6	1	6.111
6.67	485	4.67	1.3	0.00311	1	-	-	-	5.97

Here, v is the average flow velocity (m/s), d_h is the hydraulic diameter (m), ρ is the density of the water (kg/m^3) and μ is the dynamic viscosity of water $(kg/(m*s))$. For the flowframe setup, the hydraulic diameter $d_h \approx 5.2mm = 0.0052m$, the water density of the solutions is approximately $\rho = 1050kg/m^3$, the dynamic viscosity of water at 293K is $\mu = 0.001\frac{kg}{m*s}$ [31] and the velocity depends on the flow measurement. The final Reynolds numbers per flow rate are shown in Table 4.2 as Re. Under all measured flow rates, a laminar flow $(Re < 2000)$ is observed [70].

In Figure 4.7, the influence of flow rate on the diffusion boundary layer of a BPM is measured. The EIS data obtained from these measurements are processed and shown in Table 4.2. From this figure, it is clearly visible that the second semi-circle decreases at higher flow rates. This suggests that the diffusion boundary layer is indeed influenced by the difference in flow rate.

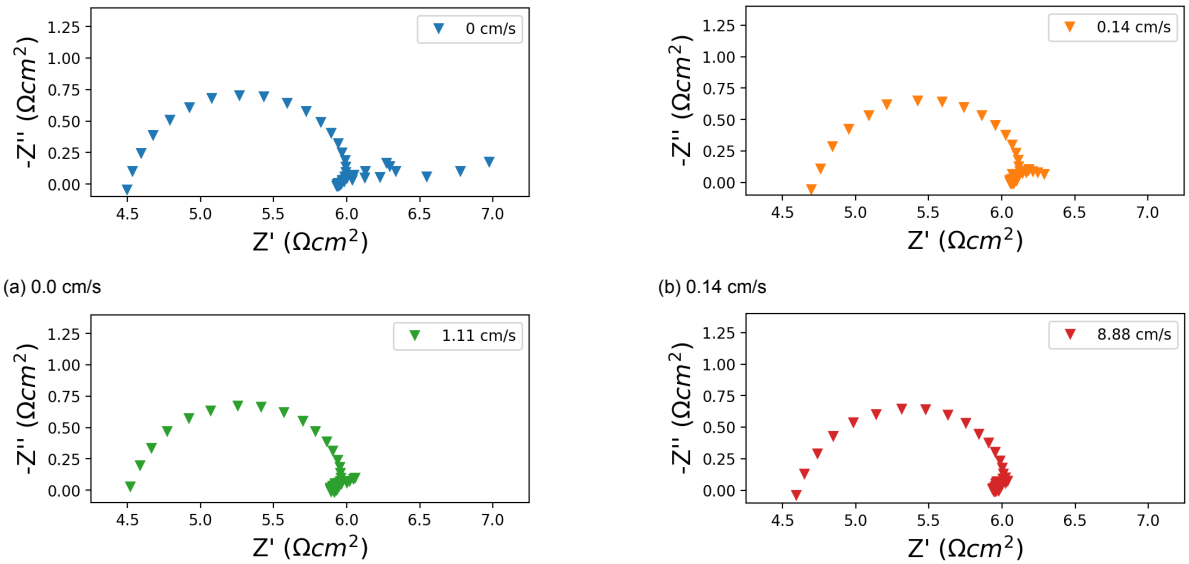

(a) 0.0 cm/s

(b) 0.14 cm/s

(c) 1.11cm/s

(d) 8.88 cm/s

Figure 4.7: EIS of a BPM under different flow rates -8.0 mA/cm^2 (water association/ forward bias).

An overview of the resistance of the DBL (R_{DBL}) versus the flow rate is shown in Figure 4.8.
In case of higher flow rates, the DBL is refreshed more and the resistance R_{DBL} decreases. Since the DBL is a layer with a different concentration of specific ions than the bulk solutions (as explained in subsection 2.2.3) and can be influenced by more refreshing, this is also in line with the hypothesis of section 4.1. At relatively higher current densities, the DBL resistance goes down. This can be caused by the enrichment of H^+ and OH^- ions in the DBL in case of water association. In case of water dissociation, the depletion of ions in the DBL can cause a higher DBL resistance, because a lack of ions in water can increase the resistance.

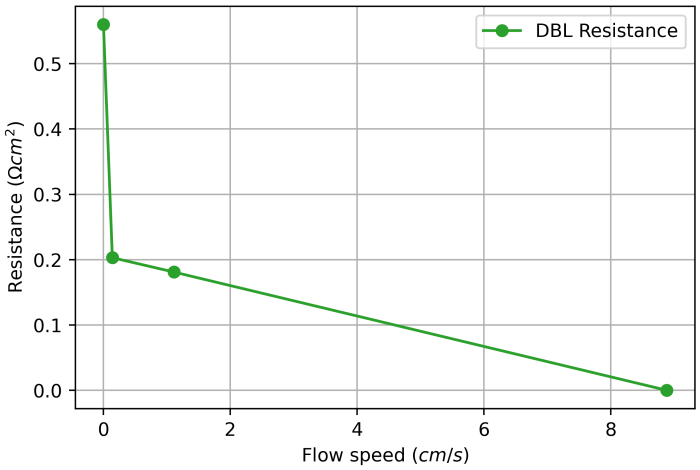

Figure 4.8: Resistance of the DBL as a function of flow rate.

4.3. EIS of single membranes

Before a whole triplet can be analysed, first every membrane has to be analysed independently. To keep water association and water dissociation separate, the membranes are measured either during water association or water dissociation.

All single membrane measurements are with a background current of $\pm 6.0 mA/cm^2$ and an EIS amplitude of 50% of the background current.

In Figure 4.9, three membranes are measured independently from each other under association and dissociation, and an EIS fitting is applied. This EIS fitting has been done by the Python script of Appendix A and the equivalent circuits of monopolar and bipolar membranes, as shown in section 4.3 and section 4.4.

Whilst associating water, the anion exchange membrane (AEM) is measured in Figure 4.9a, the bipolar membrane (BPM) is measured in Figure 4.9c and the cation exchange membrane (CEM) is measured in Figure 4.9e.

The AEM and CEM during water association are only showing one semi-circle, reflecting the non-ohmic resistance of the diffusion boundary layer (DBL) adjacent to the membrane, whilst the BPM shows with two semi-circles the water association reaction as well as the DBL. The resistances are shown in Table 4.3, according to the illustration of Figure 2.8 and Figure 2.10.

During water dissociation, the anion exchange membrane (AEM) is measured in Figure 4.9b. The bipolar membrane (BPM) is measured in Figure 4.9d and the cation exchange membrane (CEM) is measured in Figure 4.9f. The resistances are presented in Table 4.4.

The AEM during dissociation shows almost no diffusion boundary layer, whilst the CEM still shows a small semi-circle. The BPM shows a clear water dissociation reaction with a first semi-circle. The diffusion boundary layer is only very small in the second semi-circle.

The measurement of the AEM during water dissociation Figure 4.9b only shows a very small variation, without any semi-circle. This could be expected, because Figure 4.2 also shows very little effect of the DBL under $-6.0 mA/cm^2$ under water dissociation. However, it is contradictory to the CEM measurement in the same figure, since this membrane shows a semi-circle.

For the measurement of the CEM during water dissociation, as shown in Figure 4.9f, the observed semi-circle is not a perfect arc. There seems to be a small dip in the graph around $Z' = 11.2 \Omega cm^2$. This can be caused by the effect of a second RC circuit, as shown in section 4.3, although this is not expected at such high concentrations of solutions.

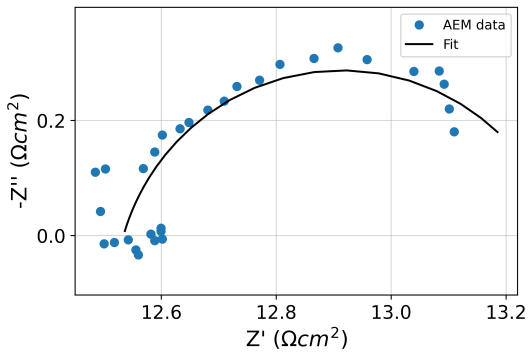

(a) AEM whilst water association (forward bias)

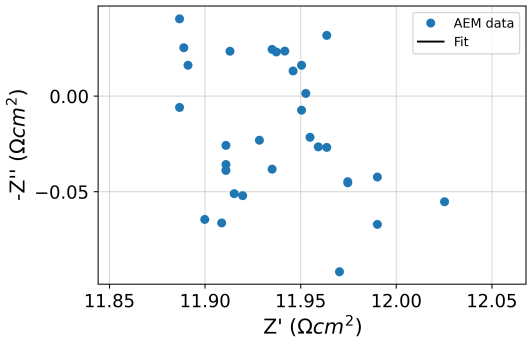

(b) AEM whilst water dissociation (reverse bias)

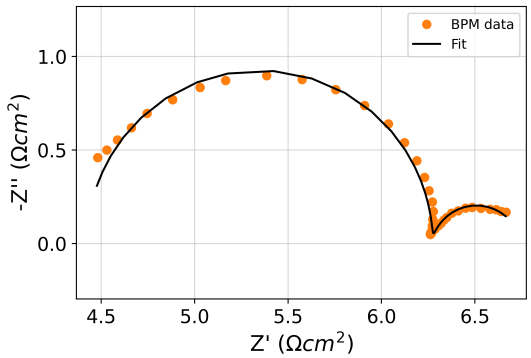

(c) BPM whilst water association (forward bias)

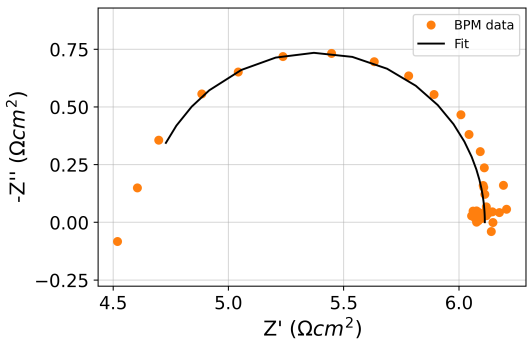

(d) BPM whilst water dissociation (reverse bias)

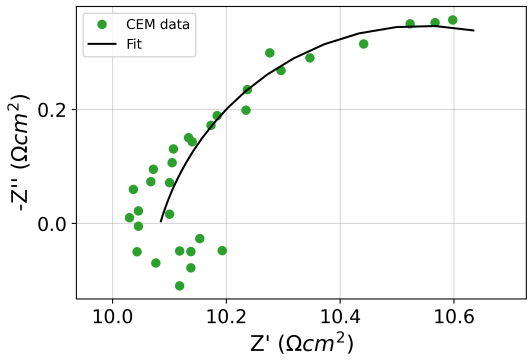

(e) CEM whilst water association (forward bias)

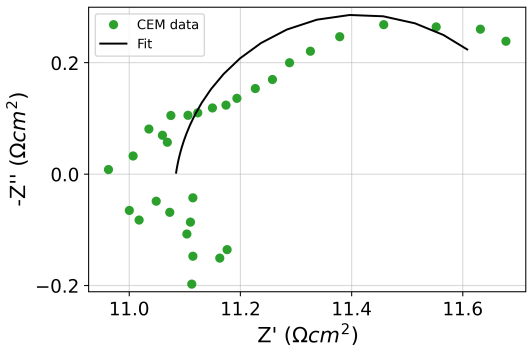

(f) CEM whilst water dissociation (reverse bias)

Figure 4.9: EIS of single membranes including a fit, with a background current of -6.0 mA/cm2 (water association) or 6.0 mA/cm2 (water dissociation)

The EIS data of Figure 4.9 contains some noise. According to Elsøe et al. [30], this noise can be explained by the AC amplitude during the measurement. For the EIS measurements of Figure 4.9, an AC amplitude of 50% of the DC background current is used. Another hypothesis for the noise in the EIS data could be that the flow inside the stack contributes to some disturbances. Although a laminar flow is observed, as discussed in subsection 4.2.1, noise could be induced by the flow or pumping pulsation.

4.4. EIS of membranes in series

In this section, three membranes in series are measured with EIS at a background current of $\pm 6.0 mA/cm^2$. This measurement has been done by putting reference electrodes in the salt compartments of an acid-base flow battery, with one triplet of AEM, BPM and CEM in between (as discussed in section 3.4). This measurement will be compared to a calculated triplet resistance, based on single membrane measurements of section 4.3.

Whilst associating water, Figure 4.10a shows the measurements of the single membranes, measured triplet and the calculated triplet (sum). This calculated triplet is calculated by taking the sum of the (non-)ohmic resistances of the single membranes in series at the same frequencies, whilst the phase shift in the Bode plot is calculated by taking the average phase shifts of the single membrane values.

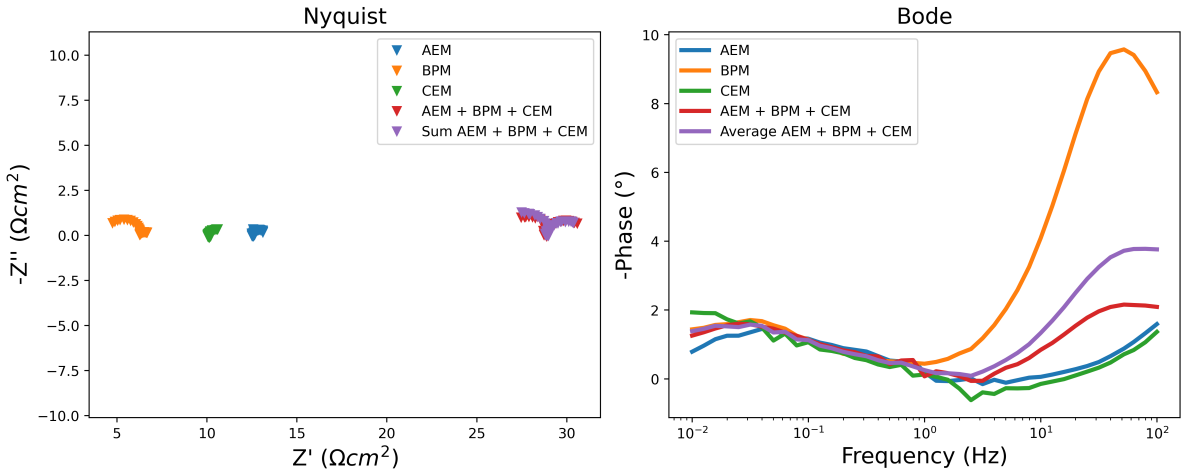

(a) Water association/ forward bias (-6.0 mA/cm^2)

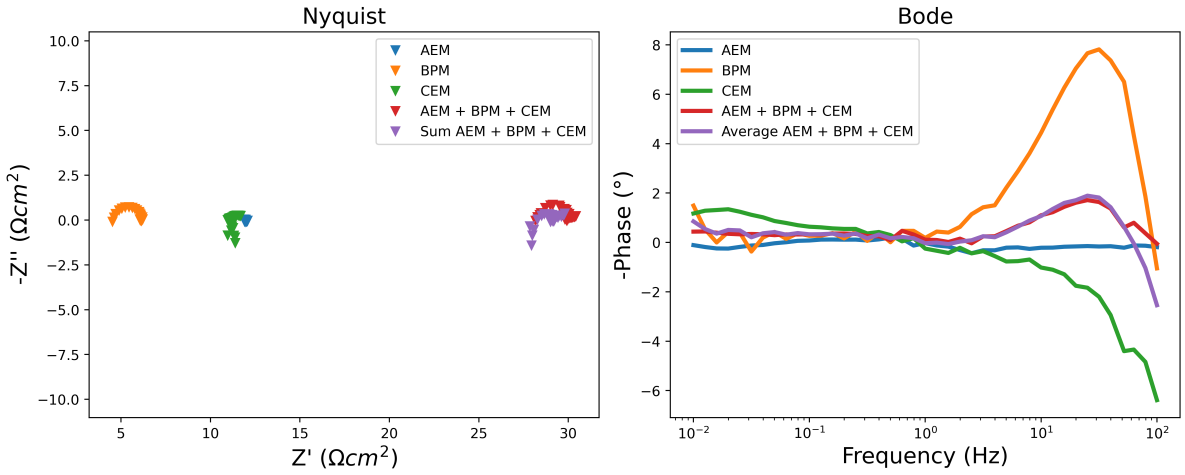

(b) Water dissociation/ reverse bias (6.0 mA/cm^2)

Figure 4.10: EIS of a triplet whist associating and dissociating water, including a measured and summed triplet.

The figure clearly shows that the measured and calculated triplet are very close to each other in the plot and seem to overlap. Figure 4.11 focuses on the measured and summed plots in forward bias. Here, it is very clear that the plots are very close to each other. The values of the measured and calculated triplet are shown in Table 4.3.

This means that during water association, the measured EIS data of a whole triplet is the sum of the three single membranes in series at the same frequencies.

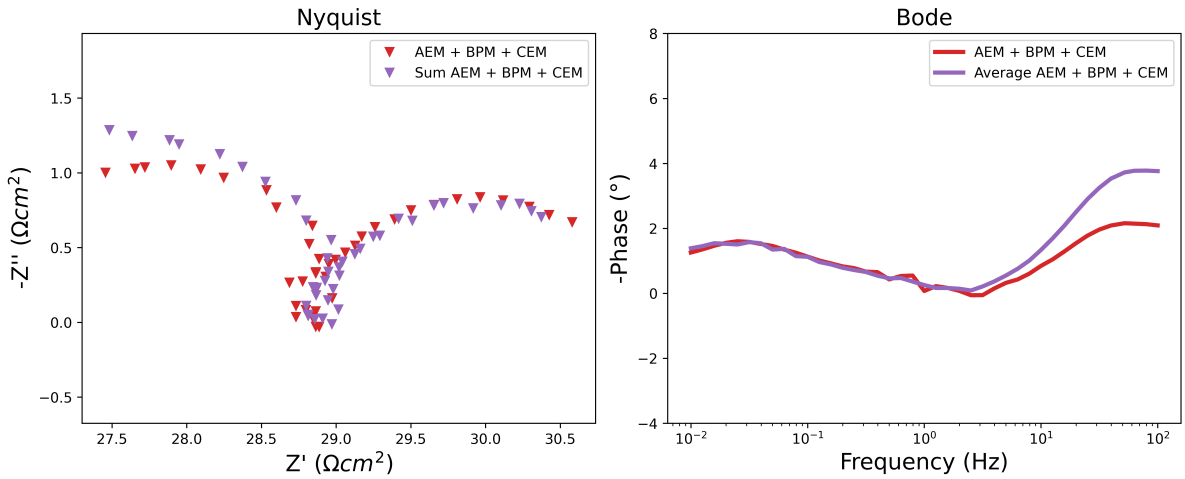

Figure 4.11: EIS of a measured and summed triplet whist associating water.

Table 4.3: Resistances of single membranes and multiple membranes in series, with a background current of -6.0 mA/cm^2 (water association) as shown in Figure 4.10a

Membrane	R_{system} [Ω cm^2]	R_{WAR} [Ω cm^2]	Q_{WAR} [F cm^2]	R_{DBL} [Ω cm^2]	Q_{DBL} [F cm^2]	n_{DBL}
AEM	12.5	-	-	0.761	4.01	0.824
BPM	4.42	1.85	0.00200	0.474	10.1	0.898
CEM	10.1	-	-	0.924	8.19	0.821
Measured	26.7	2.11	0.00128	2.16	2.03	0.844
Sum	26.4	2.51	0.000883	2.14	2.17	0.811

Figure 4.10b shows the results of single membranes whilst dissociating water, including a measured triplet and a calculated triplet (sum of membranes in series). The calculated and measured triplets have the same shapes, but the absolute values differ. The values of the water dissociating triplet are shown in Table 4.4.

Table 4.4: Resistances of single membranes and multiple membranes in series, with a background current of 6.0 mA/cm^2 (water dissociation) as shown in Figure 4.10b

Membrane	R_{system} [Ω cm^2]	R_{WDR} [Ω cm^2]	Q_{WDR} [F cm^2]	R_{DBL} [Ω cm^2]	Q_{DBL} [F cm^2]	n_{DBL}
AEM	11.9	-	-	0.016	9.54	0.000
BPM	4.62	1.48	0.00385	0.0717	10.66	0.963
CEM	11.1	-	-	0.660	8.63	0.909
Measured	28.2	1.70	0.00317	0.620	5.96	0.763
Sum	28.4	0.677	0.0099	0.772	6.44	0.853

However, the sum of the AEM, BPM and CEM during water dissociation, as shown in Figure 4.10b, is not exactly the same as the EIS measurement of the triplet. In case of water association, the measurement and summed single membranes are very close to each other. For water dissociation that seems to be different. For this phenomenon, there are two explanations. First of all, the measurements of the single membranes were not executed in the same run. Therefore, there might be slight differences in the measurement setup or it could be the case that some salt (NaCl) was still in the system for one of the measurements. Second, the location of the reference electrode might have moved a fraction, the concentration of the solutions might have changed minimally, but this would have effected the system resistance and this seams not the case, since the main difference can be found in R_{WDR}.

The resistance of the solutions for a whole triplet measurement can be calculated using Equation 3.4 of section 3.4. In this equation, the length of the solutions is $L = 3.6mm$, because this is the thickness of the flowframes plus the thickness of the 40% compressed gaskets. This concludes to a total solution resistance of $R_{\text{solutions}} = 0.543\Omega$.

This solution resistance is around 2% of the system resistance R of a triplet, which means that the majority of the resistance comes from the ohmic membrane resistance and the setup resistance (reference electrodes, wires, etc.).

A loop appeared in the Nyquist plots after multiple charge and discharge cycles, as shown in the measured triplet data of Figure 4.12a. This phenomenon is described in literature for solid state LTI lithium-ion batteries as an inductive loop formation, which appears after multiple charge-discharge cycles, as shown in Figure 4.12b [11]. Brandstätter et al. [11] states that this phenomenon in lithium-ion batteries occurs due to springs, reference electrodes, drift and corrosion and does not see any interrelationship between inductive loops and Solid Electrolyte Interphase (SEI). However, no physical springs are present in the flowframe stack, but it could have to do with reference electrodes, drift or corrosion. Also, Brandstätter et al. [11] states that in their opinion, in many cases the loops in the low-frequency range are wrongly called inductive and can be explained by a negative capacitance effect.

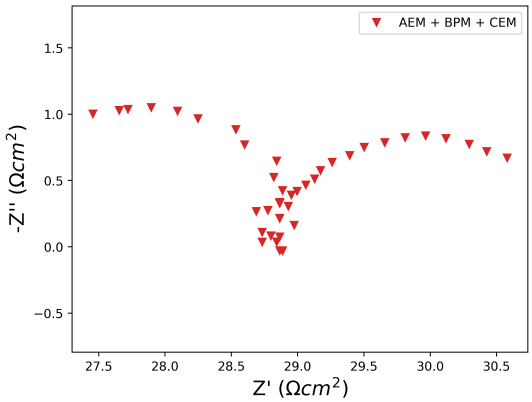

(a) Final triplet measurement (-6.0 mA/cm^2)

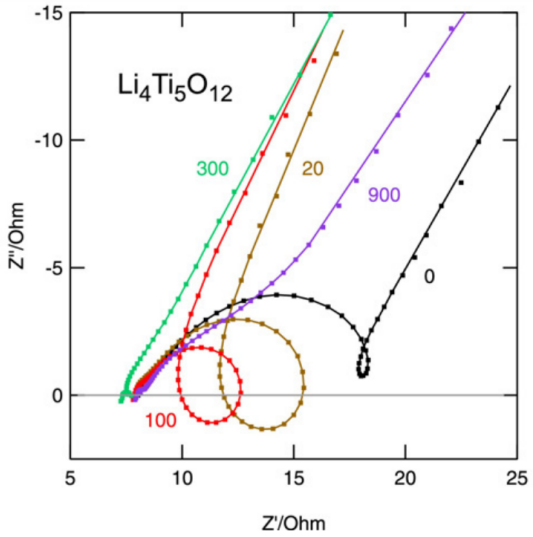

(b) Inductive loop from literature [11]

Figure 4.12: Nyquist plots of impedance data with inductive loops from a) The final triplet measurement of this research and b) a LTO lithium-ion battery with an indication of charge-discharge cycles [11]

4.5. Simplified equivalent circuit

One of the sub questions of this research is: Is it possible to compose a simplified equivalent circuit of multiple ion-exchange membranes in series, by using Electrochemical Impedance Spectroscopy data?

In this section, a simplified equivalent circuit will be conducted during association and dissociation of water, from measurements of one whole acid-base flow battery triplet.

As shown in Figure 4.10, a whole triplet can be measured using EIS and an EIS fit can be applied. The measured triplet is showing two semi-circles after an offset from the y-axis. The offset from the y-axis is due to the ohmic resistance of the system resistance including the membrane resistance, solution resistance, reference electrode resistance and other ohmic resistances in the system. The first semi-circle of the triplet measurement is due to the Water Dissociation Reaction or Water Association Reaction, because the semi-circle is very close to the first semi-circle of the BPM. The second semi-circle is due to the diffusion boundary layers of the AEM, BPM and CEM summed up in series.

For a whole triplet during water association and dissociation, Figure 5.2 shows the proposed EIS fits. From these triplet measurement fittings, a simplified equivalent circuit can be conducted and is shown in Figure 4.13. This simplified equivalent circuit resembles a double Randles cell. This Randles cell has an offset R_{system}, which represents the ohmic resistance of the system, including the ohmic resistance of the membrane and the resistance of the solutions, reference electrodes and wires [9]. The first RC circuit, is caused by the WDR inside the BPM. This reaction causes a non-ohmic resistance (R_{WDR} and Q_{DL}) and is found back in the triplet measurements. Finally, the second semi-circle, represents a larger diffusion boundary layer resistance R_{DBL} and Q_{DBL} than a BPM. The AEM and CEM have diffusion boundary layers which will add up to this final measured boundary layer (non-)ohmic resistance.

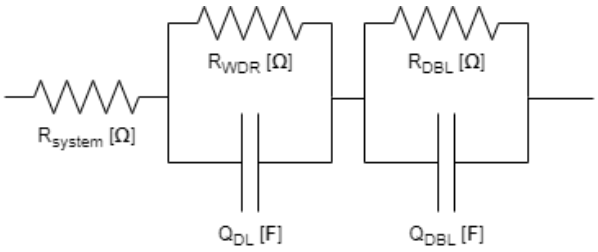

Figure 4.13: Simplified equivalent circuit for a whole ABFB triplet

Using this method, the non-ohmic resistance of a stack can be measured and used as a more accurate way for resistance calculations. The equations to obtain the resistance and capacitance are shown in section 2.4.

Because EIS shows the resistances of individual components of the membrane, a better stack can be designed and optimised, using these values. In case the DBL resistance is dominant, design changes to improve mixing can be implemented to decrease this resistance if necessary.

In Figure 4.14b, the schematic equivalent circuit during water association at -6.0 mA/cm^2 is shown including the corresponding values for the resistance and capacitance. This figure shows a system resistance including the ohmic resistance of the membrane and the resistance of the solutions, reference electrodes and wires [9].

The total resistance during water association is $R_{\text{total}} = 30.97\Omega$. The ohmic resistance (system resistance) is responsible for $R_{\text{ohmic}} = 86.2\%$ of the total resistance, whilst the non-ohmic part (WDR and DBL) counts for $R_{\text{non-ohmic}} = 13.8\%$ of the total resistance.

During water dissociation, these numbers are different. The total resistance is $R_{\text{total}} = 30.52\Omega$, but the ohmic part of counts for $R_{\text{ohmic}} \rightarrow 92.4\%$ and non-ohmic part counts for $R_{\text{ohmic}} \rightarrow 7.6\%$.

Especially the DBL resistance becomes smaller during water dissociation compared to water association. This phenomenon is also shown in Figure 4.3.

The resistance of all three solutions according to Equation 3.4 in section 3.4, is equal to $R_{\text{solutions}} = 0.54\Omega$ and is only around 1.7% of the total resistance of this stack.

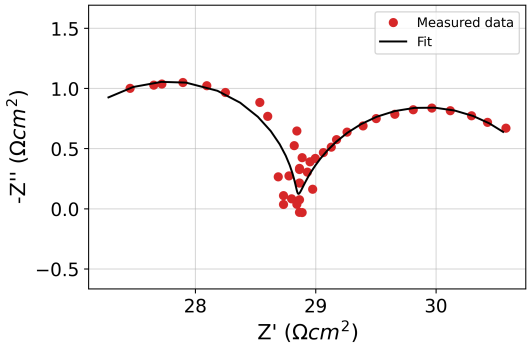

(a) Water association/ forward bias (-6.0 mA/cm^2)

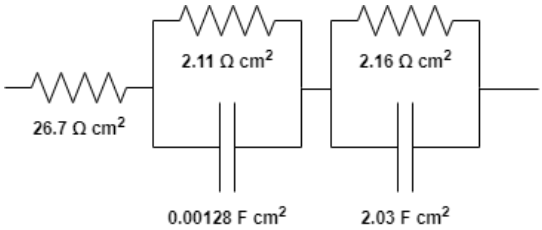

(b) Schematic equivalent circuit during water association (-6.0 mA/cm^2)

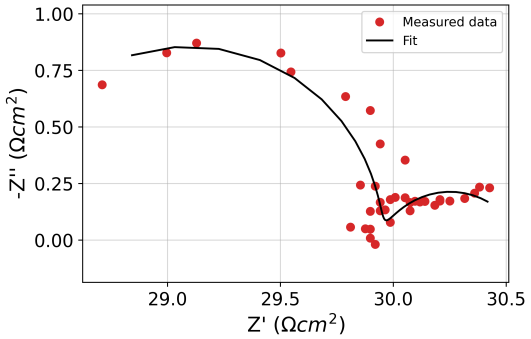

(c) Water dissociation/ reverse bias (6.0 mA/cm^2)

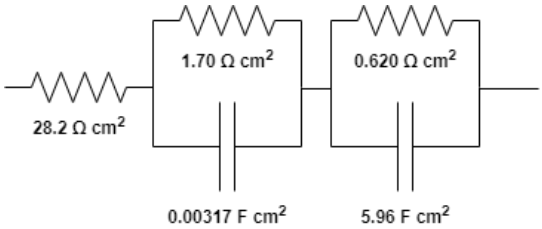

(d) Schematic equivalent circuit during water dissociation (6.0 mA/cm^2)

Figure 4.14: EIS of a triplet measurement during water association and dissociation

5

Conclusion and recommendations

The aim of this research was to analyse the non-ohmic resistance of multiple ion-exchange membranes in series. To find the answer to this aim, the following two sub-questions were formulated:

1. What is the effect of different current densities on the ohmic and non-ohmic resistance of bipolar membranes, under forward and reverse bias for electrochemical impedance spectroscopy?
2. Is it possible to compose a simplified equivalent circuit of multiple ion-exchange membranes in series, by using Electrochemical Impedance Spectroscopy data?

5.1. Conclusion

The conclusion to the first sub-question can be observed from Figure 4.3, and for the sake of clarity recalled here in Figure 5.1. As the current density of the background current increases, the total resistance and predominantly the effect of the diffusion boundary layer (DBL) resistance, becomes smaller. This plot follows an exponential decline with respect to the current density.

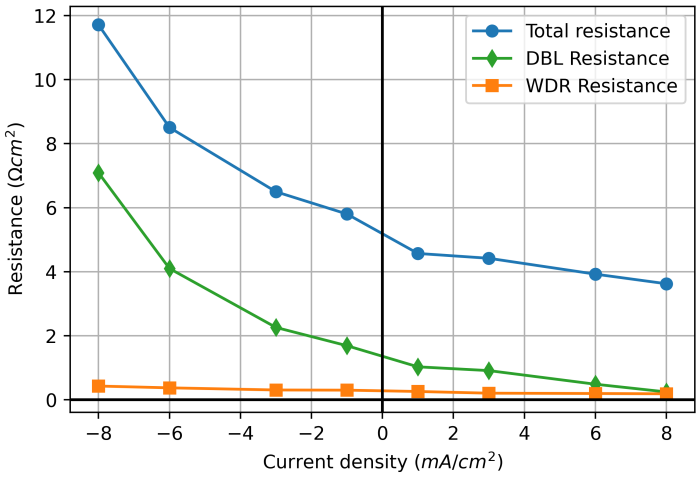

Figure 5.1: Bipolar membrane resistances as function of the current density

The hypothesis for this phenomenon was that the DBL of the bipolar membrane (BPM) gets enriched or depleted by ions and that this would influence the resistance of the DBL at the surface of the membrane.

This hypothesis is validated by multiple flow rate measurements. Increasing the flow rate in a flowframe, mixes the boundary layers adjacent to the membrane more. EIS measurements with different flow rates confirmed that the resistance of the DBL decreases, when the concentration inside the DBL changes due to higher flow rates. This affirms that the boundary layer of the BPM gets enriched or depleted by ions, due to water association and water dissociation.

The second sub-question asks if it would be possible to compose a simplified equivalent circuit out of EIS data. With multiple measurements of single membranes and hereafter, a measurement of a whole triplet, it became clear that this is indeed the case, as can be obtained from Figure 4.10a and Figure 4.13 in section 4.4 and recalled here in Figure 5.2.

The anion exchange membrane (AEM) and cation exchange membrane (CEM) only show an ohmic system resistance and a non-ohmic diffusion boundary layer (DBL). On the other hand, the BPM has an ohmic system resistance, non-ohmic water dissociation reaction (WDR) and a non-ohmic DBL.

From the measurement of the AEM, BPM and CEM in series, as presented in Figure 5.2a, it became clear that the WDR in the BPM causes a resistance and capacitance in the triplet measurements. Also, the DBL of the AEM and CEM summed with the DBL of the BPM, would construct the total resistance out of the resistances of all DBL in a triplet measurement. This summed EIS plot overlaps with the plot of a triplet measurement, as presented in Figure 5.2a shows. In the end, it was possible to conduct a simplified equivalent circuit from a whole triplet measurement, as shown in Figure 5.2b.

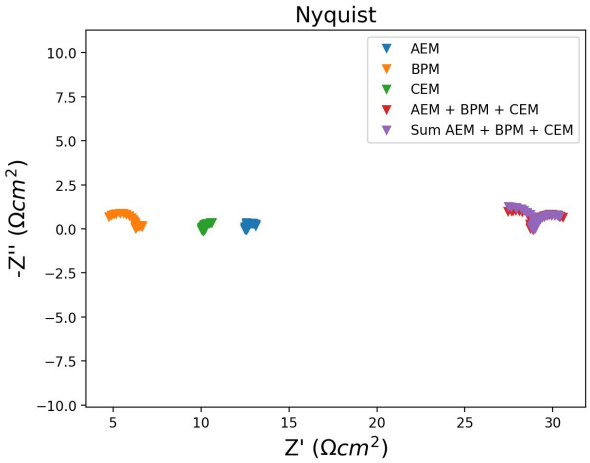

(a) EIS measurement water association/ forward bias (-6.0 mA/cm^2)

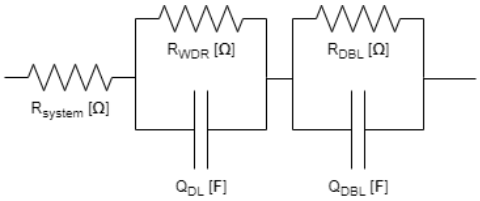

(b) Simplified equivalent circuit whole triplet

Figure 5.2: a) Nyquist plot of an EIS of a triplet measurement during water association and b) a simplified equivalent circuit for a whole triplet

In Figure 5.2b, an ohmic system resistance R_{system} describes the ohmic resistance of all solutions, membranes and measuring equipment of the triplet. The water dissociation/association reaction resistance R_{WDR} and non-ideal capacitor Q_{DL} resemble the non-ohmic resistance of the reaction and interlayer of the bipolar membrane. Finally, the resistance R_{DBL} and non-ideal capacitor Q_{DBL} show the effect of the diffusion boundary layers of all membrane-solution interfaces of the membranes in one ABFB triplet.

5.2. Recommendations

This section provides recommendations for further research in subsection 5.2.1 and provides advise for an acid-base flow battery in subsection 5.2.2.

5.2.1. Further research

- The EIS measurement results for a BPM under different current densities provide a very distinct and constant change of resistance. However, the cause of the decrease of the diffusion boundary layer resistance at relatively higher background currents is not fully proven yet. Further research could be done on the resistance of the diffusion boundary layer in relation to the applied current. Optical sensing methods could be used to observe the DBL under different current densities applied to the BPM.
- The capacitance might say something about the response time of an experiment. If a delay in the stack is present, the response time for a measurement might be different than expected. Further research could elaborate on the effect of capacitance on the response time of experiments.
- An inductive loop or negative capacitance effect is observed in section 4.4. Further research on this effect at an ABFB could give a better understanding of how this effect might influence the performance of the stack.
- This research shows that multiple membranes in series can be examined using EIS. It would be interesting to examine further possibilities of this measuring method. Measuring multiple triplets in series might give a better insight to the effect of multiple membranes in series.

5.2.2. Advise for an acid-base flow battery

The obtained knowledge of this research could be used in several ways for an acid-base flow battery (ABFB).

- The knowledge of the contribution of individual components of an acid-base flow battery (ABFB) stack could be implemented in a new stack design and optimisation. The impact of the diffusion boundary layer (DBL) to the total resistance can be limited by increasing the flow, as shown in Figure 4.8. The newly obtained knowledge of non-ohmic resistance could give a new perspective on the conventional anti-short circuit strategies.
- In section 4.5 is shown that a whole triplet can be measured using EIS. In this section, it is shown that parts of membrane resistances (such as WDR, DBL and system resistance) can be summed under their specific frequency. This knowledge could be used to examine a (part of a) stack for trouble shooting or a check if everything works as it should.
- For this research a testing stack was designed, build and tested. However, there are different sealing options possible instead of using a full area covering gasket. Further optimisation in the sealing of the stack would be beneficial for the manufacturability and strength of a stack.

Bibliography

[1] International Energy Agency. *Data and statistics*. URL: https://www.iea.org/data-and-statistics/data-browser/?country=WORLD&fuel=CO2%20emissions&indicator=CO2BySector (visited on 07/24/2022).

[2] International Energy Agency. *Global Energy Review: CO2 Emissions in 2021*. IEA, 2018. URL: https://iea.blob.core.windows.net/assets/c3086240-732b-4f6a-89d7-db01be018f5e/GlobalEnergyReviewCO2Emissionsin2021.pdf.

[3] Ahmet Aktaş. *Advances in Clean Energy Technologies*. Academic Press, 2021. Chap. Chapter 10 - The importance of energy storage in solar and wind energy, hybrid renewable energy systems. DOI: 10.1016/B978-0-12-821221-9.00010-4.

[4] Charles K. Alexander and Matthew N.O. Sadiku. *Fundamentals of Electric Circuits*. 4th ed. McGraw-Hill, 2009. ISBN: 978–0–07–352955–4. URL: http://ce.sharif.edu/courses/93-94/1/ce121-1/resources/root/fundamentals-of-electric-circuits-4th-ed-c-alexander-m-sadiku-mcgraw-hill-2009-ww.pdf.

[5] Thomas R. Anderson, Ed Hawkins, and Philip D. Jones. *CO2, the greenhouse effect and global warming: from the pioneering work of Arrhenius and Callendar to today's Earth System Models*. Elsevier, 2016. DOI: 10.1016/j.endeavour.2016.07.002.

[6] Allen J. Bard and Larry R. Faulkner. *Electrochemical Methods - Fundamentals and Applications*. John Wiley Sons, 1944.

[7] J. Benavente et al. *Electrochemical parameters of sulfonated poly(ether ether sulfone) membranes in HCl solutions determined by impedance spectroscopy and membrane potential measurements*. 2001. DOI: 10.1016/S0167-2738(01)00913-4.

[8] Abreham Tesfaye Besha et al. *Design of Monovalent Ion Selective Membranes for Reducing the Impacts of Multivalent Ions in Reverse Electrodialysis*. 2019. DOI: 10.3390/membranes10010007.

[9] Marijn Blommaert et al. "Electrochemical impedance spectroscopy as a performance indicator of water dissociation in bipolar membranes". In: *The Royal Society of Chemistry* 7.19060 (2019). DOI: 10.1039/c9ta04592a.

[10] Marijn Blommaert et al. "Insights and Challenges for Applying Bipolar Membranes in Advanced Electrochemical Energy Systems". In: *ACS Energy Letters* (2021).

[11] Harald Brandstätter, Ilie Hanzu, and Martin Wilkening. *Myth and Reality about the Origin of Inductive Loops in Impedance Spectra of Lithium-Ion Electrodes — A Critical Experimental Approach*. 2016. DOI: 10.1016/j.electacta.2016.03.126.

[12] Christopher M.A. Brett. *Electrochemical Impedance Spectroscopy in the Characterisation and Application of Modified Electrodes for Electrochemical Sensors and Biosensors*. Molecules, 2022. DOI: 10.3390/molecules27051497.

[13] Haisheng Chen et al. *Progress in electrical energy storage system: A critical review*. Elsevier, 2008. DOI: 10.1016/j.pnsc.2008.07.014.

[14] Madalina Ciobanu et al. *Handbook of Electrochemistry*. Cynthia Zoski, 2006. Chap. Chapter 1 - Fundamentals. DOI: 10.1016/B978-0-444-51958-0.X5000-9.

[15] European Commission. *Climate Action - Paris Agreement*. URL: https://ec.europa.eu/clima/eu-action/international-action-climate-change/climate-negotiations/paris-agreement_en (visited on 07/24/2022).

[16] Andrea Culcasi. "Electrical energy storage devices based on pH and salinity gradients: modelling, experiments and piloting". In: *Università degli studi di Palermo* (2021).

[17] Andrea Culcasi et al. *On the modelling of an Acid/Base Flow Battery: An innovative electrical energy storage device based on pH and salinity gradients*. Applied Energy, 2020. DOI: 10.1016/j.apenergy.2020.115576.

[18] Arindam K. Das, Murli Manohar, and Vinod K. Shahi. *Cation-Exchange Membrane with Low Frictional Coefficient and High Limiting Current Density for Energy-Efficient Water Desalination*. 2018. DOI: 10.1021/acsomega.8b01403.

[19] Deloitte. *Energy storage: Traching the technologies that will transform the power sector*. URL: https://www2.deloitte.com/content/dam/Deloitte/us/Documents/energy-resources/us-er-energy-storage-tracking-technologies-transform-power-sector.pdf (visited on 06/22/2022).

[20] Emad Al-Dhubhani et al. "Performance of five commercial bipolar membranes under forward and reverse bias conditions for acid-base flow battery applications". In: *Journal of Membrane Science* 640.119748 (2021). ISSN: 0376-7388. DOI: 10.1016/j.memsci.2021.119748.

[21] Maryori C. Díaz-Ramírez et al. *Acid/base flow battery environmental and economic performance based on its potential service to renewables support*. Journal of Cleaner Production, 2021. DOI: 10.1016/j.jclepro.2021.129529.

[22] Piotr Długołęcki et al. *Ion conductive spacers for increased power generation in reverse electrodialysis*. 2009. DOI: 10.1016/j.memsci.2009.10.011.

[23] Piotr Długołęcki et al. *On the resistances of membrane, diffusion boundary layer and double layer in ion exchange membrane transport*. 2010. DOI: 10.1016/j.memsci.2009.11.069.

[24] Piotr Długołęcki et al. *Practical Potential of Reverse Electrodialysis As Process for Sustainable Energy Generation*. 2009. DOI: 10.1021/es9009635.

[25] Sina Ebnesajjad. *Surface Preparation of Thermoplastics, Thermosets, and Elastomers*. William Andrew Publishing, 2006. DOI: 10.1016/B978-081551523-4.50010-9.

[26] W.J. van Egmond. "Concentration Gradient Flow Batteries". In: *Wageningen University & Research* (2018). URL: https://edepot.wur.nl/444261.

[27] W.J. van Egmond et al. *Performance of an environmentally benign acid base flow battery at high energy density*. International Journal of Energy Research, 2017. DOI: 10.1002/er.3941.

[28] W.J. van Egmond et al. *The concentration gradient flow battery as electricity storage system: Technology potential and energy dissipation*. Journal of Power Sources, 2016. DOI: 10.1016/j.jpowsour.2016.05.130.

[29] Elastoproxy. *Gasket Compression Explained*. 2021. URL: https://www.elastoproxy.com/enclosure-gasket-compression/.

[30] K. Elsøe et al. *Noise Phenomena in Electrochemical Impedance Spectroscopy of Polymer Electrolyte Membrane Electrolysis Cells*. 2018. DOI: 10.1002/fuce.201800005.

[31] Engineersedge. *Water density viscosity specifications*. URL: https://www.engineersedge.com/physics/water__density_viscosity_specific_weight_13146.htm (visited on 07/23/2022).

[32] Amjed Hina Fathima and Kaliannan Palanisamy. *Hybrid-Renewable Energy Systems in Microgrids*. Woodhead Publishing, 2018. Chap. 8 - Renewable systems and energy storages for hybrid systems. DOI: 10.1016/B978-0-08-102493-5.00008-X.

[33] Flexseal. *Rubber Chemical Resistance Chart*. URL: https://www.flexseal.co.uk/wp-content/uploads/2020/05/Rubber-Chemical-Resistance-Chart-V001MAR17.pdf (visited on 07/19/2022).

[34] Morton H. Friedman. *Principles and Models of Biological Transport*. Springer-Verlag Berlin Heidelberg GmbH, 1986. DOI: 10.1007/978-3-662-02467-6.

[35] Vincent J. Frilette. *Preparation and Characterization of Bipolar Ion Exchange Membranes*. American Chemical Society, 1956. DOI: 10.1021/j150538a013.

[36] Fumatech. *On Exchange Membraness*. URL: https://www.fumatech.com/NR/rdonlyres/3DF915E1-47B5-4F43-B18A-D23F9CD9FC9D/0/FUMATECH_BWT_GmbHIon_Exchange_Membranes.pdf (visited on 07/27/2022).

[37] A.H. Gamala et al. *On the Origin of the Membrane Potential Arising Across Densely Charged Ion Exchange Membranes: How Well Does the Teorell-Meyers-Sievers Theory Work?* Journal of Membrane Science Research, 2015. DOI: 10.22079/jmsr.2016.20311.

[38] Gamry. *Potentiostat Fundamentals*. URL: https://www.gamry.com/application-notes/instrumentation/potentiostat-fundamentals/ (visited on 06/22/2022).

[39] David E. Goldberg. *Fundamentals of Chemistry - 5th edition*. The McGraw-Hill Companies, 2007.

[40] L. Gurreri et al. *CFD prediction of concentration polarization phenomena in spacer-filled channels for reverse electrodialysis*. 2014. DOI: 10.1016/j.memsci.2014.05.058.

[41] Armineh Hassanvand et al. *The Role of Ion Exchange Membranes in Membrane Capacitive Deionisation*. Membranes, 2017. DOI: 10.3390/membranes7030054.

[42] ImpedancePy. *ImpedancePy Getting Started - Python*. URL: https://impedancepy.readthedocs.io/en/latest/getting-started.html (visited on 07/29/2022).

[43] Thank-God Isaiah et al. *Life Analysis of Industrial Gas Turbines Used As a Back-Up to Renewable Energy Sources*. Procedia CIRP, 2015. DOI: 10.1016/j.procir.2015.07.053.

[44] S. Koohi-Fayegh and M.A. Rosen. *A review of energy storage types, applications and recent developments*. Journal of Energy Storage, 2019. DOI: 10.1016/j.est.2019.101047.

[45] Anton Kozmai et al. *Electrochemical Impedance Spectroscopy of Anion-Exchange Membrane AMX-Sb Fouled by Red Wine Components*. Membranes, 2021. DOI: 10.3390/membranes11010002.

[46] J.J. Krol, M. Wessling, and H. Strathmann. *Concentration polarization with monopolar ion exchange membranes: current-voltage curves and water dissociation*. 1999. DOI: 10.1016/S0376-7388(99)00133-7.

[47] N. Lakshminarayanaiah. *Transport Phenomena in Artificial Membranes*. Chem Rev., 1965. DOI: 10.1021/cr60237a001.

[48] Engineering Library. *Fastener Torque*. URL: https://engineeringlibrary.org/reference/fastener-torque-nasa-design-manual (visited on 07/19/2022).

[49] Chemistry LibreTexts. *Standard Potentials*. URL: https://chem.libretexts.org/Bookshelves/Analytical_Chemistry/Supplemental_Modules_(Analytical_Chemistry)/Electrochemistry/Redox_Potentials/Standard_Potentials (visited on 07/19/2022).

[50] *Matplotlib: Visualization with Python*.

[51] Baker McKenzie. *Battery Storage - a global enabler of the Energy Transition*. URL: https://www.bakermckenzie.com/en//-/media/files/insight/publications/2022/01/battery-storage-a-global-enabler-of-the-energy-transition.pdf (visited on 06/22/2022).

[52] Rusong Miao et al. *A Review of Bolt Tightening Force Measurement and Loosening Detection*. 2020. DOI: 10.3390/s20113165.

[53] Marina Micari et al. *Salinity Gradient Heat Engines*. Woodhead Publishing, 2022. Chap. Chapter 4 - Reverse electrodialysis heat engine (REDHE). DOI: 10.1016/B978-0-08-102847-6.00004-8.

[54] P.S.R. Murthy. *Electrical Power Systems*. Butterworth-Heinemann, 2017. Chap. Chapter 24 - Renewable Energy Sources. DOI: 10.1016/B978-0-08-101124-9.00024-3.

[55] United Nations. *Paris Agreement*. 2015. URL: https://unfccc.int/sites/default/files/english_paris_agreement.pdf.

[56] Seyed Mohammed Rezaei Niya and Mina Hoorfar. *Study of proton exchange membrane fuel cells using electrochemical impedance spectroscopy technique e A review*. 2013. DOI: 10.1016/j.jpowsour.2013.04.011.

[57] Energy Storage NL. *Over energieopslag*. URL: https://www.energystoragenl.nl/energieopslag (visited on 07/24/2022).

[58] Pandas. *User guide Pandas - Python*. URL: https://pandas.pydata.org/docs/user_guide/index.html (visited on 07/29/2022).

[59] Sankara Papavinasam. *Corrosion Control in the Oil and Gas Industry*. Vol. Chapter 8. Gulf Professional Publishing, 2014.

[60] Jin-Soo Park et al. *An electrical impedance spectroscopic (EIS) study on transport characteristics of ion-exchange membrane systems*. 2006. DOI: 10.1016/j.jcis.2006.04.040.

[61] Jin-Soo Park et al. *Characterization of BSA-fouling of ion-exchange membrane systems using a subtraction technique for lumped data*. 2004. DOI: 10.1016/j.memsci.2004.07.022.

[62] R. Pärnamäe et al. *Bipolar membranes: A review on principles, latest developments, and applications*. Journal of Membrane Science, 2020. DOI: 10.1016/j.memsci.2020.118538.

[63] Ragne Pärnamäe et al. *The acid–base flow battery: Sustainable energy storage via reversible water dissociation with bipolar membranes*. Membranes, 2020. DOI: 10.3390/membranes10120409.

[64] Mark C. Porter. *Handbook of industrial membrane technology*. Noyes Publications, 1990. URL: http://amac.md/Biblioteca/data/28/14/10/32.2.pdf.

[65] Jin Ran et al. *Ion exchange membranes: New developments and applications*. 2017. DOI: 10.1016/j.memsci.2016.09.033.

[66] R. Rosliza. *Improvement of Corrosion Resistance of Aluminium Alloy by Natural Products*. TATI University College, 2011. DOI: 10.5772/32952.

[67] Alfonso Sáez, Vincente Montiel, and Antonio Aldaz. *An Acid-Base Electrochemical Flow Battery as energy storage system*. 2016. DOI: 10.1016/j.ijhydene.2016.08.141.

[68] Toshikatsu Sata. *Ion Exchange Membranes : Preparation, Characterization, Modification and Application*. Royal Society of Chemistry, 2004. URL: https://ebookcentral-proquest-com.tudelft.idm.oclc.org/lib/delft/detail.action?docID=1185660.

[69] Ahmet Senpinar. *Exergetic, Energetic and Environmental Dimensions*. Academic Press, 2018. Chap. Chapter 2.16 - Optimization of Slope Angles of Photovoltaic Arrays for Different Seasons. DOI: 10.1016/B978-0-12-813734-5.00028-7.

[70] E. Shashi Menon. *Transmission Pipeline Calculations and Simulations Manual*. Gulf Professional Publishing, 2015. Chap. Chapter 5 - Fluid Flow in Pipes. DOI: 10.1016/B978-1-85617-830-3.00005-5.

[71] Philippe Sistat and Gérald Pourcelly. *Chronopotentiometric response of an ion-exchange membrane in the underlimiting current-range. Transport phenomena within the diffusion layers*. 1997. DOI: 10.1016/S0376-7388(96)00210-4.

[72] Yoshinobu Tanaka. *Ion Exchange Membranes (Second Edition)*. Elsevier, 2015. Chap. 17 - Bipolar Membrane Electrodialysis. DOI: 10.1016/B978-0-444-63319-4.00017-1.

[73] Yoshinobu Tanaka. *Water dissociation reaction generated in an ion exchange membrane*. Journal of Membrane Science, 2010. DOI: 10.1016/j.memsci.2010.01.010.

[74] Massachusetts Institute of Technology (MIT). *The Future of Energy Storage*. URL: https://energy.mit.edu/wp-content/uploads/2022/05/The-Future-of-Energy-Storage.pdf (visited on 06/22/2022).

[75] Govinda R. Timilsina. *Are renewable energy technologies cost competitive for electricity generation?* Elsevier, 2021. DOI: 10.1016/j.renene.2021.08.088.

[76] Andrea Trovò, Walter Zamboni, and Massimo Guarnieri. “Multichannel Electrochemical Impedance Spectroscopy and equivalent circuit synthesis of a large-scale vanadium redox flow battery”. In: *Journal of Power Sources* 493.229703 (2021). ISSN: 0378-7753. DOI: 10.1016/j.jpowsour.2021.229703.

[77] J. Veerman and D.A. Vermaas. *Sustainable Energy from Salinity Gradients*. Woodhead Publishing, 2016. Chap. 4-Reverse electrodialysis: Fundamentals. DOI: 10.1016/B978-0-08-100312-1.00004-3.

[78] David A. Vermaas. *Energy generation from mixing salt water and fresh water*. Universiteit Twente, 2013. DOI: 10.3990/1.9789036535731.

[79] David A. Vermaas, Kitty Nijmeijer, and Michel Saakes. *Double Power Densities from Salinity Gradients at Reduced Intermembrane Distance*. 2011. DOI: 10.1021/es2012758.

[80] David A. Vermaas, Michel Saakes, and Kitty Nijmeijer. *Enhanced mixing in the diffusive boundary layer for energy generation in reverse electrodialysis*. Journal of Membrane Science, 2014. DOI: 10.1016/j.memsci.2013.11.005.

[81] David A. Vermaas, Michel Saakes, and Kitty Nijmeijer. *Power generation using profiled membranes in reverse electrodialysis*. 2011. DOI: 10.1016/j.memsci.2011.09.043.

[82] David A. Vermaas, Mark Sassenburg, and Wilson A. Smith. *Photo-assisted water splitting with bipolar membrane induced pH gradients for practical solar fuel devices*. 2015. DOI: 10.1039/c5ta06315a.

[83] J.F. Walther. *Process for production of electrical energy from the neutralization of acid and base in a bipolar membrane cell, US4311771A*. 1980. URL: https://patents.google.com/patent/US4311771A/en (visited on 07/18/2022).

[84] Julia Weisser Lopez. *Membrane Characterisation - AquaBattery*. 2021.

[85] Verena van der Werf. *Analysis of a three triplet acid base flow battery and a simulation based optimization of the GreenBattery - AquaBattery*. 2022.

[86] Fu-Bao Wu, Bo Yang, and Ji-Lei Ye. *Grid-scale Energy Storage Systems and Applications*. 2019. Chap. Chapter 3 - Technologies for energy storage battery management. DOI: 10.1016/B978-0-12-815292-8.00003-4.

[87] Jiabing Xia. "Reverse Electrodialysis with Bipolar Membranes (REDBP) as an Energy Storage System". In: *Universität Stuttgart* (2018). URL: https://elib.uni-stuttgart.de/bitstream/11682/10212/1/Diss_Xia.pdf.

[88] Jiabing Xia et al. *Acid-Base Flow Battery, Based on Reverse Electrodialysis with Bi-Polar Membranes: Stack Experiments*. 2020. DOI: 10.3390/pr8010099.

[89] Jianlu Zhang et al. *Pem Fuel Cell Testing and Diagnosis*. 2013. Chap. Chapter 7 - Fuel Cell Open Circuit Voltage. DOI: 10.1016/B978-0-444-53688-4.00007-3.

[90] Wenjuan Zhang et al. *Studies on Anion Exchange Membrane and Interface Properties by Electrochemical Impedance Spectroscopy: The Role of pH*. 2021. DOI: 10.3390/membranes11100771.

[91] Zhijuan Zhao et al. *Electrochemical impedance spectroscopy and surface properties characterization of anion exchange membrane fouled by sodium dodecyl sulfate*. 2017. DOI: 10.1016/j.memsci.2017.02.037.

[92] Benjamin Zirnstein, Dietmar Schulze, and Bernhard Schartel. *Mechanical and Fire Properties of Multicomponent Flame Retardant EPDM Rubbers Using Aluminum Trihydroxide, Ammonium Polyphosphate, and Polyaniline*. 2019. DOI: 10.3390/ma12121932.

A

Python code for Electrochemical Impedance Spectroscopy

This appendix shows the Python code used for the data processing of this report, as explained in section 3.6.

```
# -*- coding: utf-8 -*-
"""
Electrochemical Impedance Spectroscopy plotter

AUTOLAB excel export to plot

Created on Thu Mar 31 18:17:13 2022
Final version: 22-06-2022

@author: Zino Kramer
z.n.kramer@student.tudelft.nl
_____________________________________________________
Download datafiles in the same folder as this python file, with the following file names:
    EIS_data1_P.xlsx
    EIS_data1_Z.xlsx
    ...

In this folder, the plots will be saved as '... .png'

Required:
    Pandas      -->  type in control window: "pip install pandas"
    Matplotlib  -->  type in control window: "pip install matplotlib"
    Math        -->  type in control window: "pip install python-math"
    Impedance   -->  type in control window: "pip install impedance"

Insert input values below.
"""
# Input:
Area_membrane= 22           # Area of the membrane in cm^2

# If Galvanostatic
Background_current=-0.132   # Background current during the EIS Measurement [A]
Amplitude_EIS=0.066         # Amplitude of measurement [A] or [V]

Max_frequency = 100         # Maximum frequency you would like to plot [Hz]

# If different background currents are used, fill out:
Background_current_1 = Background_current  # Background current [A]
Background_current_2 = Background_current  # Background current [A]
Background_current_3 = Background_current  # Background current [A]
Background_current_4 = Background_current  # Background current [A]

# _____________________________________________________

```

```
# Code
import pandas as pd
import numpy as np
import matplotlib.pyplot as plt
from impedance.models.circuits import CustomCircuit
from impedance.visualization import plot_nyquist



# Data import
try:
    data1_P = pd.read_excel('EIS_data1_P.xlsx')  # load data from data1file
    data1_Z = pd.read_excel('EIS_data1_Z.xlsx')*Area_membrane   # load data from data1file
    data1a = pd.concat([data1_P, data1_Z["Z1 /ohm"], data1_Z["Z2 /ohm"]], axis=1)
    data1 = data1a[data1a["freq. /Hz"]<=Max_frequency]
    nr_measurements=1
except:
    pass
try:
    data2_P = pd.read_excel('EIS_data2_P.xlsx')  # load data from data1file
    data2_Z = pd.read_excel('EIS_data2_Z.xlsx')*Area_membrane   # load data from data1file
    data2a = pd.concat([data2_P, data2_Z["Z1 /ohm"], data2_Z["Z2 /ohm"]], axis=1)
    data2 = data2a[data2a["freq. /Hz"]<=Max_frequency]
    nr_measurements=2
except:
    pass
try:
    data3_P = pd.read_excel('EIS_data3_P.xlsx')  # load data from data1file
    data3_Z = pd.read_excel('EIS_data3_Z.xlsx')*Area_membrane   # load data from data1file
    data3a = pd.concat([data3_P, data3_Z["Z1 /ohm"], data3_Z["Z2 /ohm"]], axis=1)
    data3 = data3a[data3a["freq. /Hz"]<=Max_frequency]
    nr_measurements=3
except:
    pass
try:
    data4_P = pd.read_excel('EIS_data4_P.xlsx')  # load data from data1file
    data4_Z = pd.read_excel('EIS_data4_Z.xlsx')*Area_membrane   # load data from data1file
    data4a = pd.concat([data4_P, data4_Z["Z1 /ohm"], data4_Z["Z2 /ohm"]], axis=1)
    data4 = data4a[data4a["freq. /Hz"]<=Max_frequency]
    nr_measurements=4
except:
    pass

# Create plots
fig,(ax1, ax2) = plt.subplots(1,2, figsize=(12,5))

# Set title
if Background_current_1<0:
    bias= 'forward bias (water association)'
elif Background_current_1==0:
    bias= 'no background current'
else:
    bias= 'reverse bias (water dissociation)'
current_1 = Background_current_1/Area_membrane*1000
# fig.suptitle(f"""EIS of AEM, BPM and CEM under {bias} ({round(current_1,3)} $mA/cm^2$)""",
    fontsize =20)

color_aem = '#1f77b4'
color_bpm = '#ff7f0e'
color_cem = '#2ca02c'
color_measured = '#d62728'
color_sum = '#9467bd'



if nr_measurements>=1:
    current_1 = Background_current_1/Area_membrane*1000
    ax1.plot(data1["Z1 /ohm"], -data1["Z2 /ohm"],'v', label= """AEM""", color= color_aem)
    ax2.plot(data1["freq. /Hz"], -data1["phi /deg"], linewidth=3, label= """AEM""", color=
    color_aem)

```

```
if nr_measurements>=2:
    current_2 = Background_current_2/Area_membrane*1000
    ax1.plot(data2["Z1 /ohm"], -data2["Z2 /ohm"],'v', label="""BPM""", color= color_bpm)
    ax2.plot(data2["freq. /Hz"], -data2["phi /deg"], linewidth=3, label= """BPM""", color=
    color_bpm)
if nr_measurements>=3:
    current_3 = Background_current_3/Area_membrane*1000
    ax1.plot(data3["Z1 /ohm"], -data3["Z2 /ohm"],'v', label= """CEM""", color= color_cem)
    ax2.plot(data3["freq. /Hz"], -data3["phi /deg"], linewidth=3, label= """CEM""", color=
    color_cem)
if nr_measurements>=4:
    current_4 = Background_current_4/Area_membrane*1000
    ax1.plot(data4["Z1 /ohm"], -data4["Z2 /ohm"],'v', label="""AEM + BPM + CEM""", color=
    color_measured)
    ax2.plot(data4["freq. /Hz"], -data4["phi /deg"], linewidth=3, label= """AEM + BPM + CEM
    """, color= color_measured)

current_sum = Background_current_1/Area_membrane*1000
datasum = data1 + data2 + data3
datasum["freq. /Hz"] = datasum["freq. /Hz"] /3
datasum["phi /deg"] = datasum["phi /deg"] /3
ax1.plot(datasum["Z1 /ohm"], -datasum["Z2 /ohm"],'v', label="""Sum AEM + BPM + CEM""", color=
     color_sum)
ax2.plot(datasum["freq. /Hz"], -datasum["phi /deg"], linewidth=3, label= """Average AEM + BPM
     + CEM""", color= color_sum)

ax1.axis('equal')
# set x-axis label
ax2.set_xlabel("Frequency (Hz)", fontsize=16)
ax1.set_xlabel("Z' (Ω$ cm^2$)", fontsize=16)
# set y-axis label
ax1.set_ylabel("""-Z'' (Ω$ cm^2$)""", fontsize=16)
ax1.set_title("Nyquist", fontsize=16)
# set legend
ax1.legend()
ax2.legend()

# make a plot with different y-axis using second axis object
# ax2.plot(data1["Frequency (Hz)"], data1["phi /deg"], linewidth=3)
ax2.set_ylabel("-Phase (°)", fontsize=16)
ax2.set_title("Bode", fontsize=16)
plt.xscale('log')

fig.tight_layout()
plt.show()
# save the plot as a file
fig.savefig(f"""EIS AEM, BPM and CEM under {bias}.png""",
    format='png',
    dpi=500,
    bbox_inches='tight')


#_____________________________________________________________________________
# IMPEDANCE FITTING

EIS_fitting_membrane = ["AEM", "CEM", "BPM", "Measured", "Sum"]
for EIS_fitting_membrane in EIS_fitting_membrane:
    # EIS Number calculation
    if EIS_fitting_membrane == "AEM":
        color= color_aem
        dataEIS=data1a
        Max_frequency = 10
        dataEIS = dataEIS[dataEIS["freq. /Hz"]<=Max_frequency]
        circuit = 'R0-p(R1,CPE1)'
        initial_guess = [12, 0.6, 4, 1]
    if EIS_fitting_membrane == "BPM":
        color= color_bpm
        dataEIS=data2a
        Max_frequency = 300
        dataEIS = dataEIS[dataEIS["freq. /Hz"]<=Max_frequency]
        circuit = 'R0-p(R2,CPE2)-p(R1,C1)'
```

```
        initial_guess = [4, 3.5, 1, 0.1, 1.8, 0.001]
    if EIS_fitting_membrane == "CEM":
        color= color_cem
        dataEIS=data3a
        Max_frequency = 10
        dataEIS = dataEIS[dataEIS["freq. /Hz"]<=Max_frequency]
        circuit = 'R0-p(R1,CPE1)'
        initial_guess = [12, 0.6, 4, 1]
    if EIS_fitting_membrane == "Measured":
        color= color_measured
        dataEIS=data4
        Max_frequency = 300
        dataEIS = dataEIS[dataEIS["freq. /Hz"]<=Max_frequency]
        circuit = 'R0-p(R2,CPE2)-p(R1,C1)'
        initial_guess = [4, 3.5, 1, 0.1, 1.8, 0.0001]
    if EIS_fitting_membrane == "Sum":
        color= color_sum
        dataEIS=datasum
        Max_frequency = 300
        dataEIS = dataEIS[dataEIS["freq. /Hz"]<=Max_frequency]
        circuit = 'R0-p(R2,CPE2)-p(R1,C1)'
        initial_guess = [4, 3.5, 1, 0.1, 1.8, 0.0001]

    frequencies = np.array(dataEIS["freq. /Hz"])
    frequencies=frequencies[::-1]

    Zi = []
    for x in dataEIS.index:
        Zi.append(complex(dataEIS["Z1 /ohm"][x],dataEIS["Z2 /ohm"][x]))
    Z = np.complex128(Zi)
    Z=Z[::-1]

    #_____________________________________________________________________________
    #Fitting impedance model circuit

    circuit = CustomCircuit(circuit, initial_guess=initial_guess)
    circuit.fit(frequencies, Z)
    print(circuit)
    #_____________________
    # print to file
    # circuit.to_excel(f"""EIS_circuit {EIS_fitting_membrane}.xlsx""")
    import sys
    original_stdout = sys.stdout
    with open(f"""EIS_circuit {EIS_fitting_membrane}.txt""", 'w') as f:
        sys.stdout = f
        print(circuit)
        sys.stdout = original_stdout

    Z_fit = circuit.predict(frequencies)
    #_____________________________________________________________________________
    #Plot graph

    fig, ax = plt.subplots()
    plot_nyquist(ax, Z, fmt='o', color = color)
    plot_nyquist(ax, Z_fit, fmt='-', color = 'k')
    plt.ylabel("""-Z'' (Ω$ cm^2$)""", fontsize=16)
    plt.xlabel("Z' (Ω$ cm^2$)", fontsize=16)
    # plt.title(f"""EIS fitting {EIS_fitting_membrane} under {bias}""", fontsize=16)
    plt.axis('equal')
    ax.set_aspect('equal')
    plt.legend([f"""{EIS_fitting_membrane} data""", 'Fit'])
    plt.show()

    fig.savefig(f"""EIS fitting {EIS_fitting_membrane} under {bias} bias.png""",
        format='png',
        dpi=500,
        bbox_inches='tight')
```

B

Equivalent circuit monopolar membranes

In this appendix, different approaches for monopolar membranes are considered, in addition to subsection 3.2.2.
In literature, different approaches for monopolar membranes appear. The reason for this is the difference in boundary layer approach.

In Figure B.1a, a monopolar cation exchange membrane with its adjacent layers is shown. The membrane itself behaves as an equivalent circuit containing R_{M}, as a resistor. Directly next to the membrane, the electrical double layer (DL) is formed. The equivalent circuit of the DL is equal to a RC circuit, having a resistor R_{DL} parallel to a capacitor C_{DL}.

From this point the Diffusion Boundary Layer (DBL) forms a second layer to the membrane, behaving as a resistor R_{DBL} parallel to a non-ideal capacitor or constant phase element (CPE) Q_{DBL} [23].

Finally, according to Piotr et al., the overview of Figure B.1 is the equivalent circuit of a monopolar membrane [23].

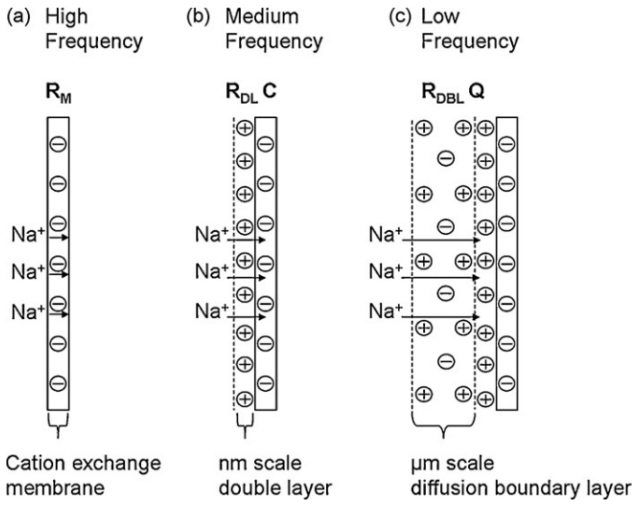

(a) Schematic monopolar membrane layers [23].

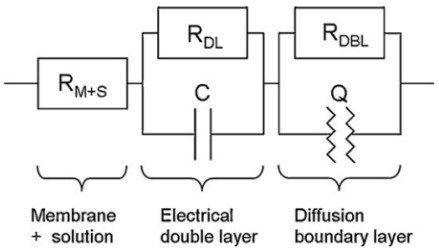

(b) Equivalent circuit monopolar exchange membrane [23]

Figure B.1: Occurring phenomena in the CEM and in the layers adjacent to the membrane. Here, R_{M} is the membrane resistance, R_{DL} is the double layer resistance with capacitor C and R_{DBL} is the diffusion boundary layer resistance with constant phase element (non-ideal capacitor) Q, according to Piotr et al. [23].

Park et al. states that monopolar membranes have two Randles cells. The first Randles cell is due to the Heterogeneous Transport (HT) and the second Randles cell shows the Diffusion Boundary Layer (DBL), as shown in Figure B.2.

However, with a 0.5 M KCL solution, one of the Randles cells was not visible anymore, as shown in Table B.1. Only with very low concentrations of salt and no stirring, the second RC circuit is detectable. Since the research in this report only uses concentrations of 0.5 M and higher, the second Randles cell seems not relevant.

Also, Gurreri et al. [40] states that at higher salt concentrations (0.5 M NaCl), the pure membrane resistance is the dominant one, the diffusion boundary layer plays a considerable role and the double layer resistance is not significant.

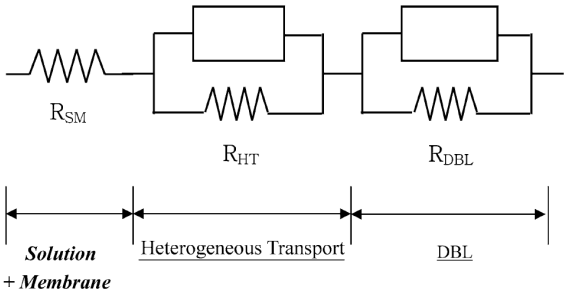

Figure B.2: Monopolar exchange membrane equivalent circuit according to Park et al.[60]

Table B.1: Values of electrochemical parameters obtained by fitting the experimental impedance data using the suggested equivalent circuit with concentration of the KCl solution and existence of stirring, according to Park et al. [60]

Solution (M KCl)	Stir-ring	R_{SM} ($\Omega\,cm^2$)	R_{HT} ($\Omega\,cm^2$)	Q_{HT}[a]		R_{DBL} ($\Omega\,cm^2$)	Q_{DBL}[a]	
				$Y^*_{0,HT}$	n		$Y^*_{0,DBL}$	n
0.01	No	134.6	42.59	1.883	1.0	17.60	0.231	0.59
	Yes	135.9	26.16	0.358	0.79	–	–	–
0.025	No	50.29	15.01	5.981	1.0	9.467	0.578	0.53
0.5	No	6.476	0.793	16.29	0.73	–	–	–
	Yes	6.585	0.375	13.55	0.70	–	–	–

Note. Subscript SM, effects of the membrane immersed in solution; HT, effects of heterogeneous transport; DBL, effects of diffusion boundary layer.

[a] The dimensions are S s^n/cm^2; if $n = 1$, they are F/cm^2.

Kozmai et al. and Trovò et al. state that the equivalent circuit of an anion exchange membrane (AEM) is equal to a single Randles cell [45] [76].

Since the goal of this research is to examine the effect of multiple ion-exchange membranes in series and all solutions next to the monopolar membranes are 0.5 M or higher and stirred/with flow, the single Randles cell model of Figure B.3 is chosen for this report. For a more detailed representation of monopolar membranes, a double Randles cell representation can be a better option.

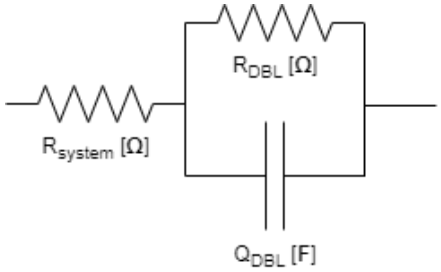

Figure B.3: Equivalent circuit of a monopolar exchange membrane, used for this report

C

Instructions EIS at flowframe stack using an AUTOLAB potentiostat

This appendix shows instructions of how to use the flowframe setup using the AUTOLAB potentiostat at Delft University of Technology.

C.1. Small Flowframe Setup

The flowframe setup is shown in Figure C.1, with the working electrode on the right-hand side of the figure. A schematic overview is given in Figure C.2.

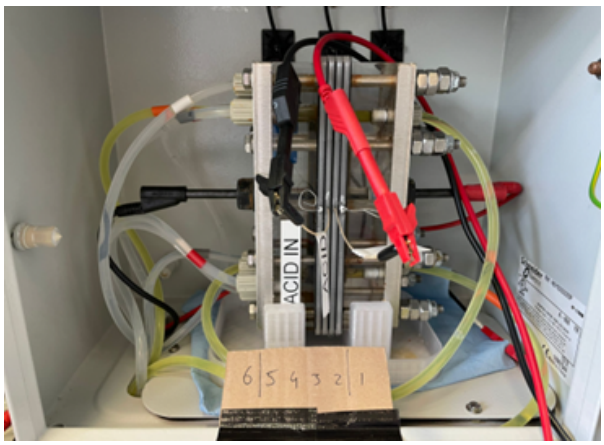

Figure C.1: Flowframe Setup overview with working electrode on the right-hand side.

This setup is build out of flowframes, with a mesh inside the flowframes for a proper flow distribution. This is shown in Figure C.3.

C.1.1. Tubing

For the flowframe setup, the bottom connections are the inlets and the upper connections are the outlets, as can be observed in Figure C.4.

From and to the stacks, the tubes are arranged and colour coded as shown in Figure C.5 and Table C.1

C.1.2. Reference electrodes

To measure the potential over one or more membranes, there are two 1.0 mm reference electrodes (RE) available. One RE is marked as ACID and one is marked as BASE. Because Ag/AgCl REs can degrade in base solutions, make sure you use this RE in BASE solutions. Whilst inserting the

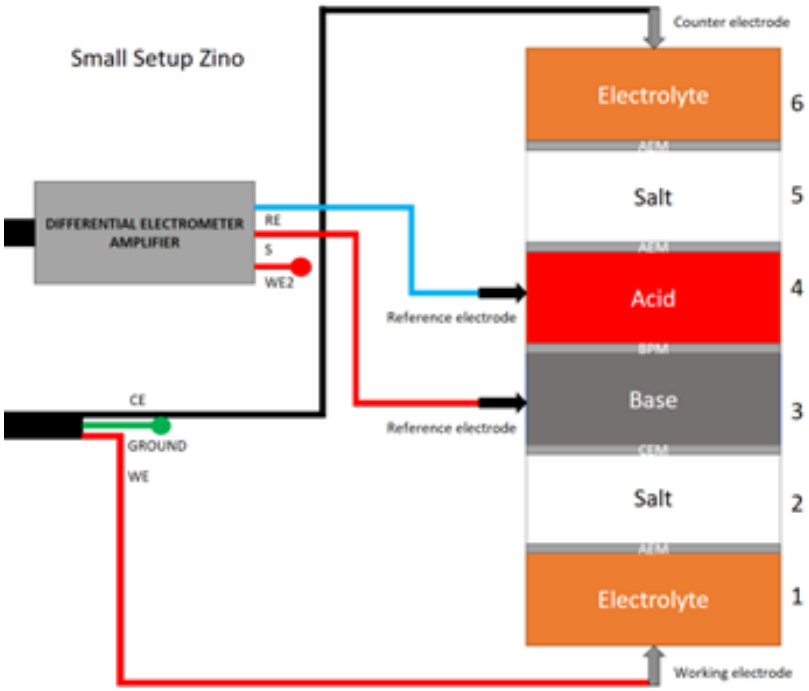

Figure C.2: Schematic overview flowframe setup.

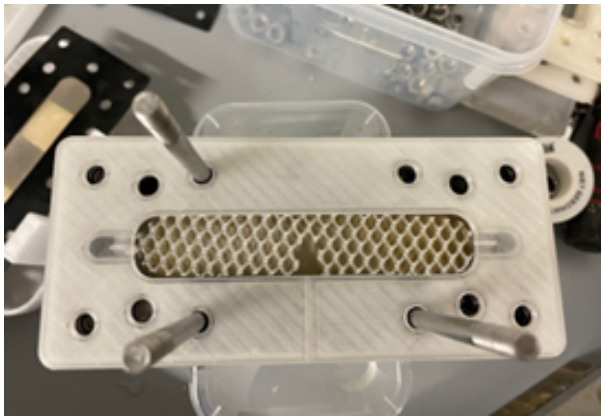

Figure C.3: Inside the flowframes.

Table C.1: Colour coding flowframe setup AUTOLAB.

Colour	Compartment	Solution
White	2, 5	Salt
Grey	3	Base
Red	4	Acid
Orange	1, 6	Electrolyte height

reference electrodes, make sure you insert the electrode gently until the black mark on the electrodes. If you push further, there might be a chance of puncturing the tip of the REs by hitting the mesh (as shown in Figure C.3).

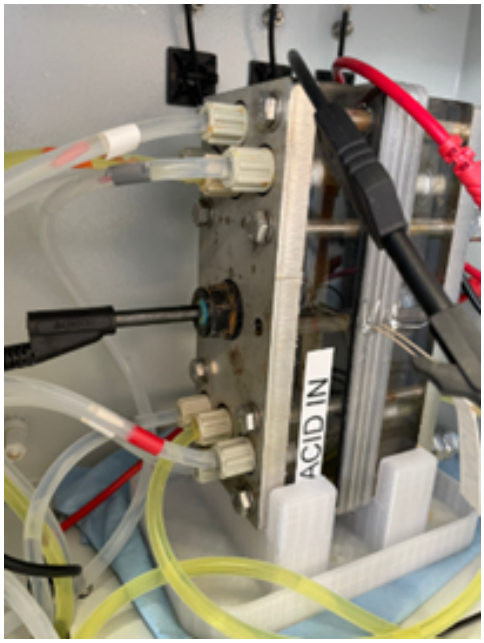

Figure C.4: Inlets (bottom) and outlets (top) of the flowframes.

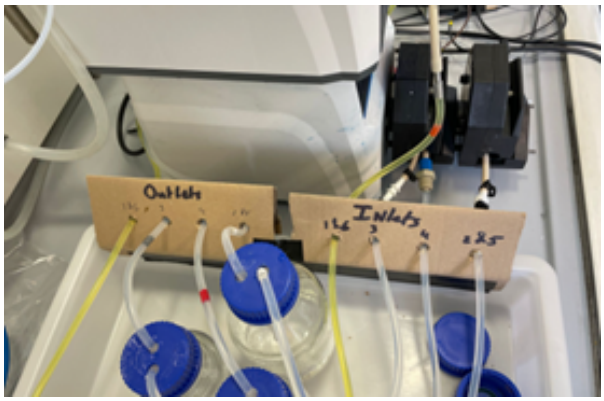

Figure C.5: Inlets and outlets tubing tray.

C.1.3. Clean setup

To clean the setup, please drain the system and flush it once with distilled water. The reference electrodes can be taken out of the flowframes, rinsed with distilled water, the caps on the tips and put back in the corresponding bags. To make sure the system will not leak, put the iron wire back in the reference electrode holes. If they leak too much, you can use white Teflon tape to make it leak-tighter. To preserve the (bipolar) membranes, please pump 0.5 M NaCl inside the system when the experiments are done.

C.2. Hardware EIS

To start with EIS, the following is required:

- Potentiostat (AUTOLAB is used in this appendix)
- Computer with software of the potentiostat
- Setup for your specimen

C.2.1. Potentiostat

The AUTOLAB potentiostat (Figure C.6) is used for this appendix. This potentiostat uses two large cables with 6 smaller cables in total, to connect your testing setup.

Figure C.6: AUTOLAB potentiostat

The cables and settings can be tested, using the AUTOLAB DUMMYCELL 2 (Figure C.7).

Figure C.7: DUMMYCELL 2 AUTOLAB

C.2.2. Flowframe setup

In lab E1.090 of Delft University of Technology, there is a 6-compartment cell setup, to measure impedance (Figure C.8).

In this cell, a membrane can be placed in the middle of the setup, by lowering the lever and detaching the “magnifying glass”-shaped holder. Mind that there are O-rings, which should stay in place. By opening the holder, a membrane can be applied. When the holder and specimen are ready, the holder can be placed back in the cell and the lever can be pushed up again. This cell is connected to the peristaltic pumps, which should be put in bottles with according solutions. Make sure that no dangerous gasses are being produced at the working or counter electrode. For example, in the setup of Figure C.9 a bipolar membrane is inserted in the holder in the cell. An acid and base are used at either side of the membrane. To connect the cables to the test cell, follow the guidelines according to the overview of Figure C.9.

C.2.3. Software

For AUTOLAB, use the Nova software of Figure C.10.

In this software, the AUTOLAB potentiostat will automatically connect if the potentiostat is ON and connected, using USB (Figure C.11).

Click “Open library” to start a new task. For Impedance, choose “FRA impedance potentiostatic” to perform impedance with alternating voltage and choose “FRA impedance galvanostatic” to perform

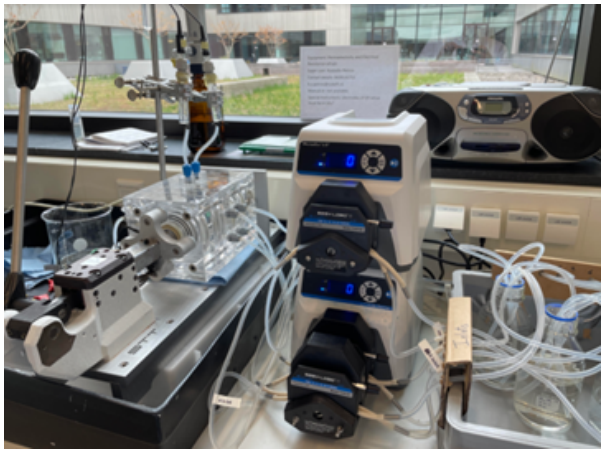

Figure C.8: 6-compartment cell for EIS

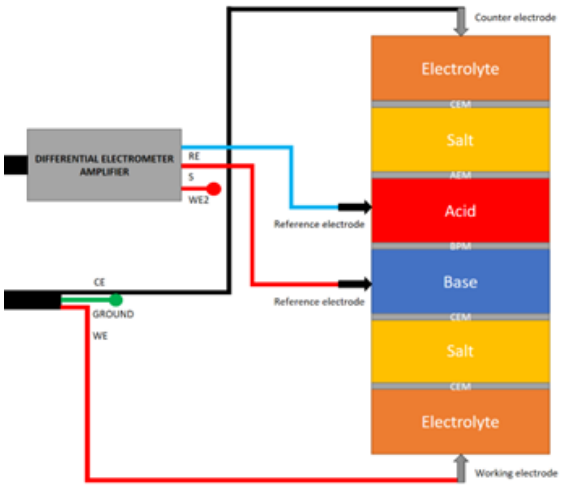

Figure C.9: Cables overview EIS

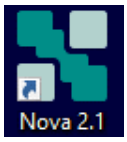

Figure C.10: NOVA logo

impedance with alternating current (Figure C.12). If you want to apply a background voltage, you also have to use an alternating voltage (potentiostatic). For current, vice versa (galvanostatic).

For a good impedance measurement, you have to adjust some settings. Most of the time, the amplitude of the measurement has to be at 50% of the background current/voltage to avoid noise in the lower frequencies (as shown in Figure C.13). The frequency range is dependent of your research. However, for the current setup a measurement between 1000Hz and 0,01Hz would be the most reliable without any background noise.

Do not forget to TURN OFF the pumps, before performing EIS. Otherwise, noise will occur in the lower frequencies.

C.2.4. Data processing

To export data from the AUTOLAB software, you double click on the impedance graph, click on the matrix symbol, and export as Excel file (Figure C.14).

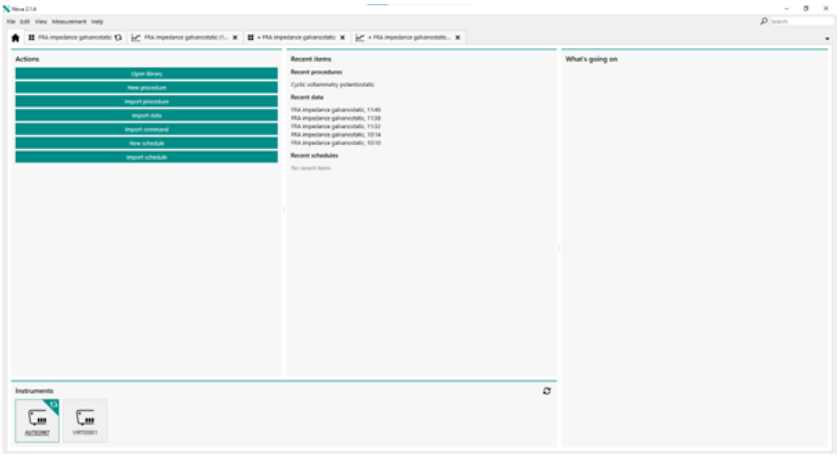

Figure C.11: Start NOVA

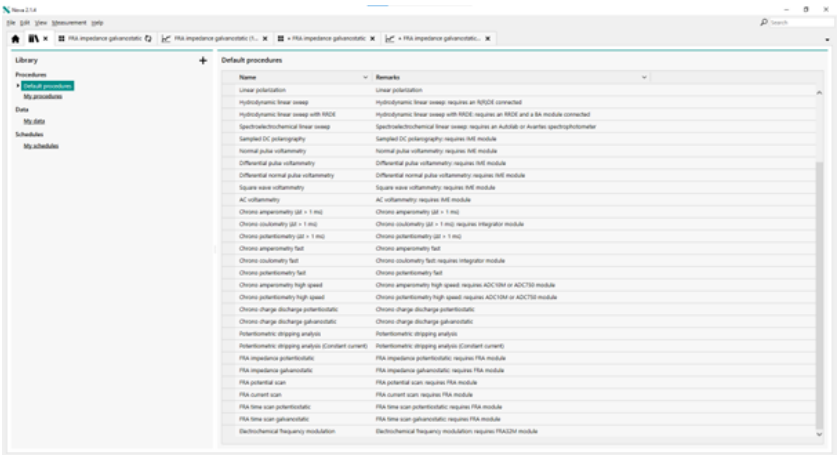

Figure C.12: Choose FRA impedance potentiostatic or galvanostatic

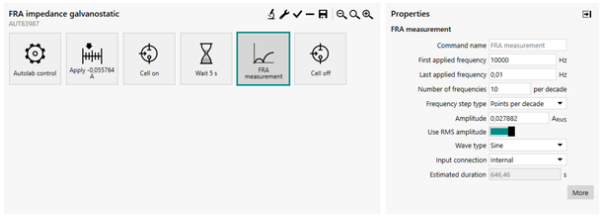

Figure C.13: NOVA example settings EIS

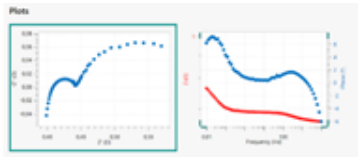

(a) Step 1 exporting data

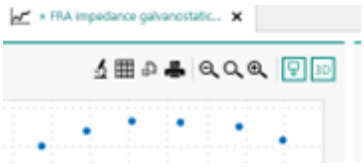

(b) Step 2 exporting data

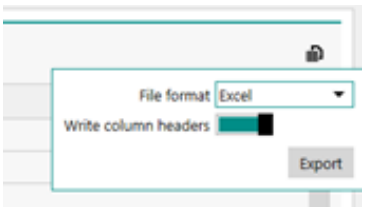

(c) Step 3 exporting data

Figure C.14: Export data steps NOVA AUTOLAB

Use this data to create a plot in excel, or use a Python script for this (as shown in Appendix A).